General Disclaimer

One or more of the Following Statements may affect this Document

- This document has been reproduced from the best copy furnished by the organizational source. It is being released in the interest of making available as much information as possible.

- This document may contain data, which exceeds the sheet parameters. It was furnished in this condition by the organizational source and is the best copy available.

- This document may contain tone-on-tone or color graphs, charts and/or pictures, which have been reproduced in black and white.

- This document is paginated as submitted by the original source.

- Portions of this document are not fully legible due to the historical nature of some of the material. However, it is the best reproduction available from the original submission.

Produced by the NASA Center for Aerospace Information (CASI)

FZA-434-2
31 Aug 1968
VOLUME 2

FACILITY FORM 602

N69-11253
(ACCESSION NUMBER)

(THRU)

98
(PAGES)

1
(CODE)

CR-98112
(NASA CR OR TMX OR AD NUMBER)

31
(CATEGORY)

PARAMETRIC STUDY of OPTIMIZED LIQUID-HYDROGEN THERMAL PROTECTION SYSTEMS for NUCLEAR INTERPLANETARY SPACECRAFT

Technical Details

GENERAL DYNAMICS
Fort Worth Division

GENERAL DYNAMICS
Fort Worth Division

FZA-434-2
31 August 1968

PARAMETRIC STUDY OF OPTIMIZED LIQUID-HYDROGEN THERMAL PROTECTION SYSTEMS FOR NUCLEAR INTERPLANETARY SPACECRAFT

Volume 2. Technical Details

Prepared for the
George C. Marshall Space Flight Center
National Aeronautics and Space Administration
Huntsville, Alabama

under

Contract NAS8-21080

Prepared by:

D. G. Barry
Sr. Aerothermodynamics Engineer

T. S. Hunter
Aerothermodynamics Engineer

Approved by:

R. A. Stevens
Aerothermodynamics Group Engineer

GENERAL DYNAMICS
Fort Worth Division

PRECEDING PAGE BLANK NOT FILMED.

F O R E W O R D

This document is Volume 2 of the final report on Contract NAS8-21080, "An Analytical Study of Storage of Liquid-Hydrogen Propellant for Nuclear Interplanetary Spacecraft." The study was performed by the Fort Worth Division of General Dynamics Corporation for the George C. Marshall Space Flight Center of the National Aeronautics and Space Administration. The program was conducted under the technical direction of Mr. D. Price of the MSFC Propulsion and Vehicle Engineering Laboratory. His assistance in the performance of the study is gratefully acknowledged.

The final report comprises three volumes:

Volume 1. Results and Summary

Volume 2. Technical Details

Volume 3. Numerical Data

Volume 1 contains a complete presentation and discussion of the results together with a summary of the important findings of the study. Volume 2 contains a description of the methods of analysis and the computer programs used in the study. Volume 3 contains a tabulation of the numerical data, including both the thermal protection system optimization results and the mass-buildup data.

The authors would like to acknowledge the contributions of K. A. Pinter and M. K. Fox in the mission analysis tasks and of L. E. Heyduck, Jr., in the structural and meteoroid protection analyses.

PRECEDING PAGE BLANK NOT FILMED.

TABLE OF CONTENTS

		Page
	FOREWORD	iii
	LIST OF FIGURES	vii
	LIST OF TABLES	ix
	NOTATION	xi
1.	INTRODUCTION	1
2.	MISSION ANALYSIS	3
	2.1 Mission Definition	3
	2.2 Energy Requirements	8
	2.3 Mars Orbit Analyses	9
3.	VEHICLE DEFINITION	23
	3.1 Nuclear Propulsion Module	23
	3.2 Conjunction-Class Mars Vehicle	26
	3.3 Mars Excursion Module Analysis	32
	3.4 Mass Buildup Data	37
4.	THERMAL ANALYSIS	39
	4.1 Thermal Model	40
	4.2 Thermal Environment Evaluation	41
	4.3 Penetration Heat Transfer	44
5.	STRUCTURAL ANALYSIS	47
	5.1 Tank Mass Equation	47
	5.2 Meteoroid Protection Requirements	49

TABLE OF CONTENTS (Cont'd)

	Page
6. OPTIMIZATION METHODS	57
6.1 Preliminary Analysis	60
6.2 Final Analysis Computer Program	66
APPENDIX A: VENT PRESSURE ANALYSIS	73
APPENDIX B: STRESS ANALYSIS	79
REFERENCES	83

LIST OF FIGURES

Figure	Title	Page
2.1-1	Heliocentric Mission Geometry	6
2.1-2	Variation of Solar Distance with Flight Time	7
2.3-1	Martian Atmosphere Density Models	13
2.3-2	Variation of Orbit Decay Rates with Altitude	14
2.3-3	ΔV Requirements for Mars Braking and Departure vs Altitude	15
2.3-4	Variation of Maximum Orbit Inclination with Altitude	16
2.3-5	Mars Orbit Orientation Analysis: h_{Mars} = 9203 n.mi	17
2.3-6	Mars Orbit Orientation Analysis: h_{Mars} = 3238 n.mi	18
2.3-7	Mars Orbit Orientation History: h_{Mars} = 9203 n.mi	19
2.3-8	Mars Orbit Orientation History: h_{Mars} = 3238 n.mi	20
2.3-9	Mars Orbit Orientation History: h_{Mars} = 216 n.mi	21
3.1-1	Nuclear Propulsion Module	25
3.2-1	Conjunction-Class Mars Vehicle	30
3.2-2	Mars Transfer Solar Shield-Vehicle Configuration	31
3.2-3	Mars Orbit Solar Shield-Vehicle Configuration	31

L I S T O F F I G U R E S (Cont'd)

Figure	Title	Page
3.3-1	MEM Deorbit Entry Conditions	35
3.3-2	Variation of MEM Mass with Altitude	36
5.2-1	Meteoroid Protection Requirements: $P_o = 0.995$	54
5.2-2	Multi-Wall Effectiveness Factors	55
A-1	Effect of Vent Pressure on Optimum Total Effective Mass Fraction: Mars Departure Stage	75
A-2	Effect of Vent Pressure on Optimum Total Effective Mass Fraction: Mars Departure Stage, NPSP = 5.0 psia	76
A-3	Effect of Vent Pressure on IMIEO and Propellant Storage Penalty: Mars Departure Stage	77
A-4	Effect of Vent Pressure on IMIEO and Propellant Storage Penalty: Mars Braking Stage	78

LIST OF TABLES

Table	Title	Page
2.1-1	Mission Summary	5
3.2-1	Nominal Stage Mass Fractions	29
3.3-1	Mars Excursion Module Mass Buildup	34
3.4-1	Miscellaneous Component Masses	37
4.2-1	Comparison of Earth-Orbit Adiabatic Wall Temperatures	41
4.2-2	Average Inclination to Terminator for Mars Orbit	43
4.2-3	Average Absorbed Heat Flux for Mars Orbit	43
5.2-1	Meteoroid Parameters	51
5.2-2	Meteoroid Protection Area Densities	53

PRECEDING PAGE BLANK NOT FILMED.

NOTATION

A - area, also boiloff mass fraction (ratio of boiloff mass to total propellant loading)

A_o - area of both tank ends

a - semi-major axis of the ellipsoidal tank ends, also "a factor" as defined in Section 6

B - area density

B_{max} - Brinell hardness

b - semi-minor axis of the ellipsoidal tank ends

C - a constant in the linear scaling equation, also a constant coefficient in the saturation pressure curve-fit equation

C_D - drag coefficient

c_t - speed of sound

D - the tank diameter

d - meteoroid diameter, also "d factor" defined in Section 6

E - mass fraction (ratio of mass to total propellant loading)

e - eccentricity of the ellipsoidal tank ends

F - the view factor for radiation heat transfer

F_c - contingency factor

F_S - safety factor

f - a factor to allow for area dependent penetrations, also stress

f_t - tensile stress

h_{fg} - latent heat of vaporization

k - thermal conductivity of the insulation

ℓ - total tank length (including heads)

M - mass

M_o - Initial Mass in Earth Orbit

M.S. - margin of safety

m - meteoroid mass

N - number of meteoroids, also total number of mission phases

n - ratio of the maximum vehicle acceleration to the standard acceleration due to gravity

n_o - a control number

P - probability, also tank pressure

ΔP - pressure increment required by the NPSP of the pump

P_s - vapor pressure of saturated liquid hydrogen

p - penetration depth

ΔQ - heat transfer during a given time period

$\dot{Q}_p$ - penetration heat transfer rate

$\dot{q}$ - heat flux

R - specific gas constant for hydrogen

r - fraction reliquified in a partial-recondensation system

S - solar constant

T - time, also absolute temperature

$\overline{T}_{log}$ - log mean of inlet-gas and liquid-hydrogen temperatures

$(\overline{\Delta T})$ - time average temperature difference across the insulation

t - tank wall thickness

u - specific internal energy of saturated liquid hydrogen

V - meteoroid velocity, also tank volume

Y - a generalized mass

α - parameter in meteoroid flux equation, also absorptance

β - parameter in meteoroid flux equation, also symbol for a collection of terms in the tank mass equation

γ - constant term in the saturation pressure curve-fit equation

δ - insulation thickness

ϵ - emissivity

η - fraction of a mission phase during which boiloff occurs

θ - time duration of a mission phase

μ - ullage fraction

ρ - density, also saturated liquid hydrogen density

σ - ultimate tensile strength, also Stefan-Boltzmann constant

ϕ - meteoroid flux

Subscripts

bo - boiloff

c - coating

E - exposed area

H - hydrogen

i - insulation

j - stage identification

k - mission phase identification

m - meteoroid, also node identification

max - maximum

mod - module

mp - meteoroid protection

n - node identification

o - initial condition

p - pressurant

s - saturated liquid hydrogen condition

t - tank

u - useful

y - pertaining to mass Y

θ - mission phase θ

SECTION 1

INTRODUCTION

This volume presents a detailed discussion of the analysis methods and the computer programs used in this study. The analytical effort required support from three different areas: mission analysis, structural analysis, and thermal analysis. Discussion in this volume is oriented toward these individual areas and shows how each contributes to the optimization analysis of the propellant storage system. In addition, Section 3 is devoted to a description of the Mars vehicle including the basic nuclear propulsion module, the Mars Excursion Module, and associated mass data required for a complete mass-buildup of the vehicle.

The optimization techniques used in this study are treated in Section 6. This discussion presents the basic technique and a description of the computer programs used in the preliminary and the final phases of this study.

PRECEDING PAGE BLANK NOT FILMED.

SECTION 2

MISSION ANALYSIS

Investigation of space vehicle propellant thermal protection systems requires a fairly detailed mission analysis to establish the mission time history, the heliocentric and planetocentric mission geometry, and the stage propellant loadings. In this study, the mission analysis assumed even greater importance since two of the basic parameters, Earth orbit staytime and Mars orbit altitude, are also mission parameters. In this section, the selection of the reference mission is discussed and the mission parameters are defined. The analyses concerning Mars orbit altitude and orientation are also described.

2.1 MISSION DEFINITION

The reference mission for this study is a conjunction-class manned Mars stopover mission. Conjunction-class missions are so named because conjunction of Mars occurs approximately midway between the Earth departure date and the Earth arrival date. This class of missions is characterized by long mission durations (about 2½ years from Earth departure to Earth arrival), long staytimes at Mars (about 1½ years), relatively low energy requirements (when compared to other Mars mission classes), relatively small variations in energy requirements from year to year, and relatively low unbraked entry speeds at Earth arrival. These low Earth entry speeds make it possible to omit an Earth braking stage, thereby reducing the amount of propellant which must be thermally protected during the mission.

Conjunction-class missions can be divided on the basis of the transfer angle of each leg of the mission. The particular mission selected for this study has transfer angles of less than 180 degrees for both the outbound and inbound legs of the mission. This mission type yields relatively long staytimes at Mars compared to the time spent in transit to and from the planet. It also offers the shortest mission duration among the conjunction-class missions available during a launch opportunity. Energy requirements generally exceed those corresponding to the absolute minimum energy opportunities available in the conjunction class, but the

difference is not sufficient to nullify the advantages of a shorter total mission duration and longer staytime for exploration at Mars.

The selected mission departs Earth on 1 March 1984 and returns to Earth on 17 September 1986. Mission duration following departure from Earth orbit is 930 days, and the total duration varies from 1020 to 1200 days, depending upon the Earth orbit staytime. The data in Table 2.1-1 summarize the nominal mission; the data are standard trajectory data and are self-explanatory. A two-body patched-conic approach is used for trajectory definition. Although precision trajectory determination of the mission could have been performed, the effects on the results of this study would not have been significant.

The heliocentric geometry for the mission is presented in Figure 2.1-1. This polar plot relates solar distance, heliocentric longitude and time to give a graphical representation of the mission. Variation of solar distance with elapsed time after departure from Earth orbit is presented in Figure 2.1-2 which is useful in propellant heating calculations over the interplanetary trajectory. The data for these two figures were generated by a two-body spacecraft ephemeris computer program.

TABLE 2.1-1

MISSION SUMMARY

	Civil Date	Julian Date
Depart Earth:	1.0 March 1984	244 5760.5
Arrive Mars:	27.0 September 1984	244 5970.5
Depart Mars:	19.0 February 1986	244 6480.5
Return Earth:	17.0 September 1986	244 6690.5

Outbound Flight Time:	210 days
Mars Staytime:	510 days
Inbound Flight Time:	210 days

	Planetocentric (Earth) Departure Phase	Planetocentric (Mars) Departure Phase
Parking Orbit Altitude:	262 n.mi (485 km)	Selected*
Hyperbolic Excess Speed:	0.1270 EMOS	0.0813 EMOS
Declination of Departure Asymptote:	-35.71°	9.62°
Right Ascension of Departure Asymptote:	182.43°	212.72°
Parking Orbit Inclination:	36.0°	Selected*

	Heliocentric Phase (Outbound Leg)	Heliocentric Phase (Inbound Leg)
Heliocentric Transfer Angle:	148.89°	141.77°
Inclination of Transfer Orbit:	3.53°	0.894°
Eccentricity of Transfer Orbit:	0.1835	0.2396
Perihelion Distance:	0.9621 AU (no transit)	0.9948 AU (no transit)
Aphelion Distance:	1.3946 AU	1.618 AU (no transit)

	Planetocentric (Mars) Arrival Phase	Planetocentric (Earth) Return Phase
Parking Orbit Altitude:	Selected*	Direct Reentry
Unbraked Entry Speed:	--	38,321 ft/sec (11.6801 km/sec)
Hyperbolic Excess Speed:	0.1272 EMOS	0.1235 EMOS
Declination of Arrival Asymptote:	4.51°	14.03°
Right Ascension of Arrival Asymptote:	316.53°	110.25°
Parking Orbit Inclination:	Selected*	-

* The selected circular orbit altitudes and inclinations are:

Altitude	Inclination
9203 n.mi (17,053 km)	10.7 deg
3238 n.mi (6000 km)	63.0 deg
216 n.mi (400 km)	75.2 deg

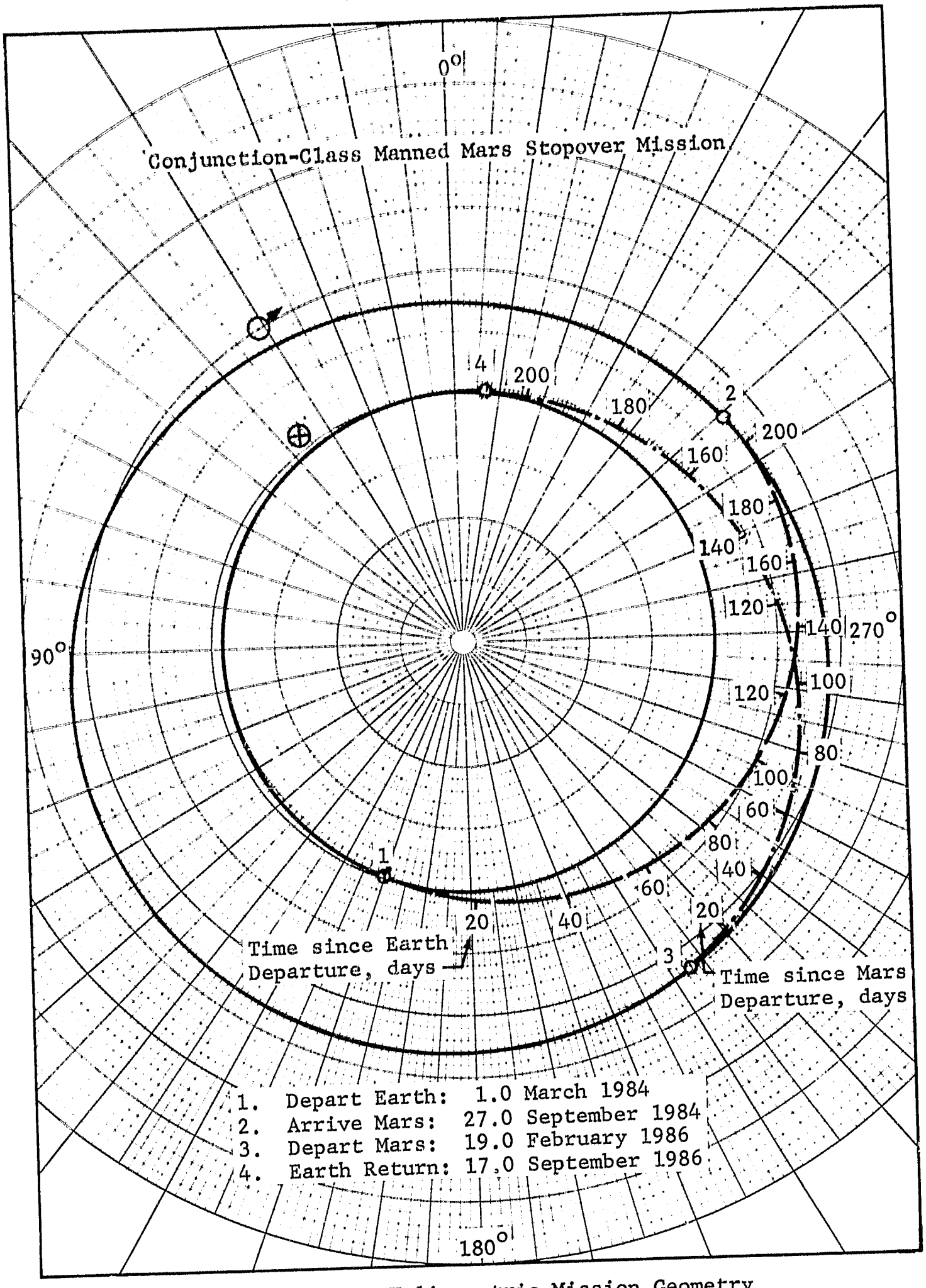

Figure 2.1-1 Heliocentric Mission Geometry

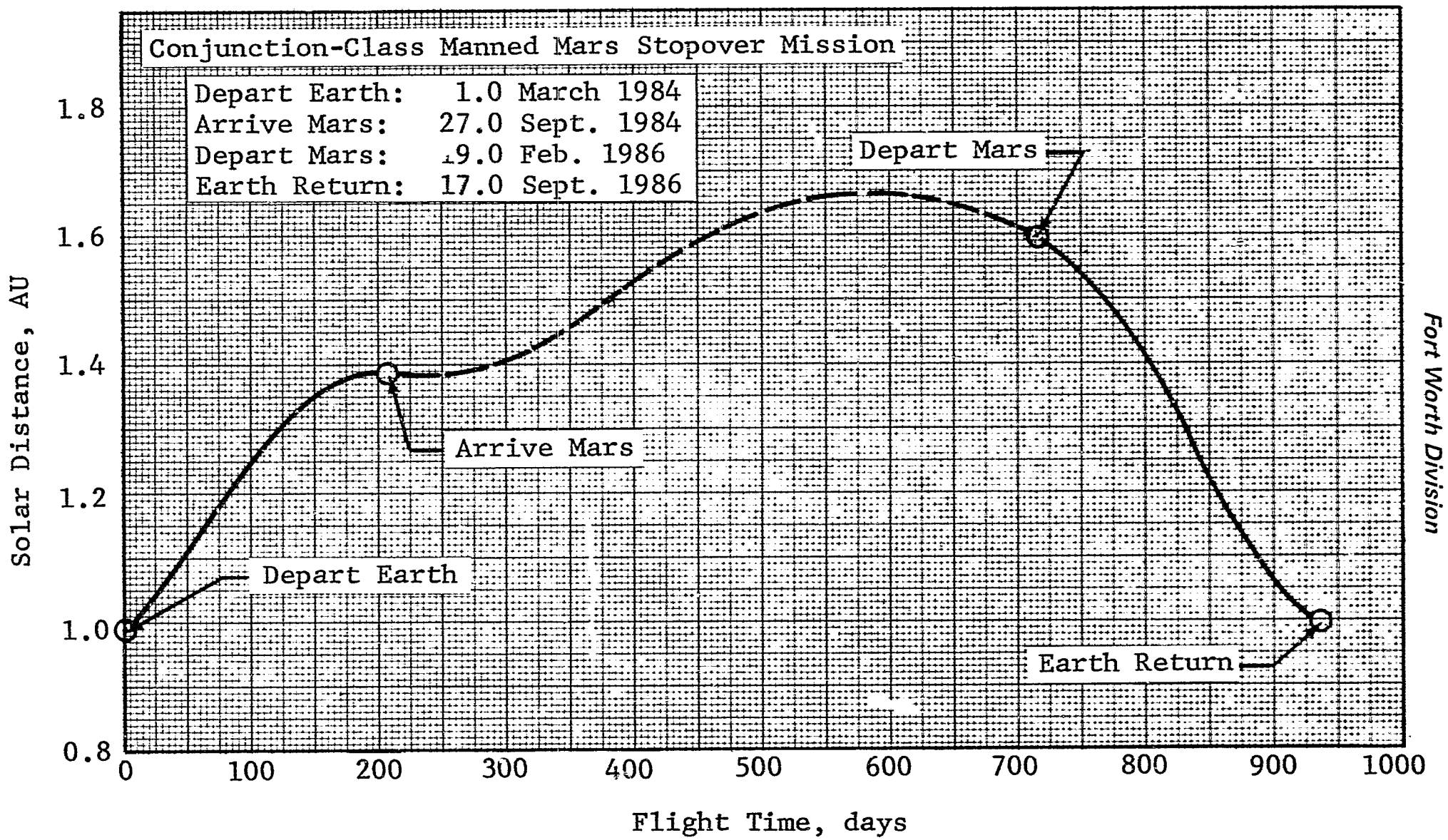

Figure 2.1-2 Variation of Solar Distance with Flight Time

GENERAL DYNAMICS
Fort Worth Division

2.2 ENERGY REQUIREMENTS

Primary mission energy requirements used for vehicle sizing were based on a 20-day launch opportunity at Earth and a 30-day departure opportunity at Mars. The effect of each opportunity was established by determining the maximum hyperbolic excess velocity across a launch period centered on the minimum ΔV mission. The effect of the launch opportunity at Earth on the energy requirements for the Mars braking stage was included. The maximum hyperbolic excess velocities are 0.14, 0.15, and 0.09 EMOS (1 EMOS = 97,657 ft/sec or 29.766 km/sec) at Earth departure, Mars braking, and Mars departure, respectively.

The propulsion velocity increments for the primary propulsion phases were computed using these hyperbolic excess velocities with allowances for gravity losses, small plane changes, and performance reserves. The gravity-loss allowances were based on data in Reference 2-1. ΔV allowances for 7-degree plane changes at Earth departure and Mars departure were included to allow for the possibility of a non-coplanar departure. A 3% ΔV performance reserve was used.

2.3 MARS ORBIT ANALYSES

2.3.1 Altitude Selection

A major task of the mission analysis was to define the range of circular-orbit altitudes at Mars. The upper altitude was specified in the groundrules to be the synchronous altitude; the lower altitude was specified on the basis of orbit lifetime considerations.

The altitude for a synchronous orbit was determined by computing the altitude of the orbit whose period is equal to the period of rotation of Mars about its axis (24 hours, 37.38 minutes). The gravitational parameter of Mars was assumed to be 1.5138175×10^{15} ft^3/sec^2 (42866.849 km^3/sec^2) and the radius of Mars was assumed to be 1826 n.mi (3381 km). The computed altitude is 9203 n.mi (17,053 km).

Primary parameters that determine the lifetime of a spacecraft in orbit about Mars are the density profile of the atmosphere and the ballistic coefficient, M/C_DA, of the spacecraft. Determination of the orbit lifetime is complicated by the large uncertainty in the actual density profile. This uncertainty is indicated in Figure 2.3-1 which presents the density profiles for the three Martian model atmospheres defined in Reference 2-2. The selection of the minimum possible circular-orbit altitude based on lifetime is not practical because of this large variation in density. Also, it is desirable to maintain the altitude within reasonable limits. Consequently, the lower altitude was selected on the basis of a small decrease in altitude for a 510-day staytime using the density profile defined by the "upper density" model of Reference 2-2. The ballistic coefficient of the spacecraft in Mars orbit was estimated by assuming a mass of 250,000 lb_m (113,400 kg), a drag coefficient of 2.0, a diameter of 33 ft (10 m), and a length of 100 ft (30.5 m). The ballistic coefficient was computed to be approximately 146 lb_m/ft^2 (712 kg/m^2) for an orientation where the vehicle longitudinal axis is parallel to the velocity vector and approximately 38 lb_m/ft^2 (185 kg/m^2) for the case where the longitudinal axis is perpendicular to the velocity vector. Orbital decay rate as a function of altitude is presented in Figure 2.3-2. The lower circular-orbit altitude was selected to be 216 n.mi (400 km); this orbit would decay less than 7 n.mi (13 km) in 510 days.

The factors considered in the selection of the intermediate orbit altitude were:

1. Variation of the ΔV for Mars braking and Mars departure with altitude.

2. Reconnaissance capability.

3. Landing site accessibility.

It was also desirable to select an intermediate altitude somewhere near the average of the upper and lower altitudes. The variation of the ΔV's for Mars braking, Mars departure, and their sum with altitude is presented in Figure 2.3-3. The sum of the ΔV's is a minimum at an altitude of approximately 3000 n.mi (5560 km). The reconnaissance capability and the landing site accessibility depend on the orbit inclination. Higher inclinations tend to allow better surface coverage and a wider range of latitudes for the landing site. Unless costly (in terms of propellant requirements) plane changes are permitted during descent to and ascent from the surface, the maximum attainable latitude is equal to the inclination of the orbit. The maximum inclination is limited by the requirement that no plane change be required at departure. The method used to determine the possible inclinations for a given altitude is described in Subsection 2.3.2. Variation of the maximum orbit inclination which allows coplanar departure with altitude is shown in Figure 2.3-4. Maximum inclination decreases rapidly as altitude increases and is less than 40 degrees for altitudes above 4000 n.mi (7400 km). The selected intermediate altitude is 3238 n.mi (6000 km). The sum of the ΔV's for Mars braking and departure is near the minimum at this altitude and the orbit inclination is greater than 60 degrees.

2.3.2 Orbit Orientation Analysis

One aspect of the mission analysis task was to generate orbit orientation histories with respect to the terminator for each of the selected parking orbits at Mars. The first step in this procedure is to compute the nodal precession rate and the second step is the selection of the orientation of the parking orbit.

The nodal precession rate, $\dot{\lambda}_p$, was determined by using the following equation:

$$\dot{\lambda}_p = \frac{-3\pi J_2}{T(R/R_o)^2} \sin \delta_p$$

where J_2 = coefficient of the second harmonic of the planet's gravitational potential

T = orbit period

R = orbit radius

R_o = planet radius

δ_p = orbit pole declination

Although this is only a first-order approximation of $\dot{\lambda}_p$, it is felt that the expression is sufficiently accurate for purposes of this study.

The criteria used to select the orbit orientation are: (1) no plane change at the time of departure, and (2) a posigrade orbit. To make this selection it is necessary to determine the loci of the arrival and departure poles. These loci, which are called pole circles, lie in planes; one locus is normal to the arrival excess velocity asymptote and the other locus is normal to the departure excess velocity asymptote. The variation of these loci with declination and right ascension is shown in Figure 2.3-5. If there were no orbital precession, the correct declination of the orbit pole (and, hence, the inclination of the orbit) for coplanar departure would be the intersection of the two pole circles. However, there is precession and the amount of precession depends on both the altitude and the declination of the orbit pole. The precession rate is very sensitive to orbit altitude. For example, the precession rates for the three selected altitudes are given below for an orbit pole declination of 90° ($J_2 = 1.989 \times 10^{-3}$).

Altitude	Precession Rate
9203 n.mi (17,053 km)	0.02866 deg/day
3238 n.mi (6000 km)	0.43716 deg/day
216 n.mi (400 km)	10.517 deg/day

The high altitude (synchronous) orbit orientation analysis is presented in Figure 2.3-5. The locus of the arrival poles after 510 days of precession were computed from a $\Delta\lambda_p$ obtained by multiplying the precession rate for a given declination by the total staytime. Intersections of the locus of precessed orbit poles with the departure pole circle define possible poles for coplanar departure. For this case, there are two possible poles, but the pole which has a negative declination can be eliminated because this orbit would be retrograde. Therefore, the only possible pole for the synchronous orbit has a declination of 79.3 degrees and an orbit inclination of 10.7 degrees.

The orbit orientation analysis for the intermediate altitude is presented in Figure 2.3-6. For this case, there are six possible poles. The poles numbered from 4 to 6 were eliminated since the orbits for these poles would be retrograde. Pole number 1 was selected because the corresponding capture orbit offers the most favorable orientation for planet reconnaissance, i.e., maximum inclination.

The high precession rate for the low altitude allows the selection of many orbit inclinations. The locus of precessed orbit poles intersects the departure pole circle at many points. Although the maximum possible inclination is nearly polar, an orbit inclination of 75.2 degrees was selected. This orbit inclination provides good surface coverage and allows the selection of a landing site over a wide range of latitudes.

A time history of the inclination of the parking orbit to the terminator for a stay time of 510 days was obtained for each of the three selected parking orbits at Mars. These data are presented in Figures 2.3-7, 2.3-8 and 2.3-9.

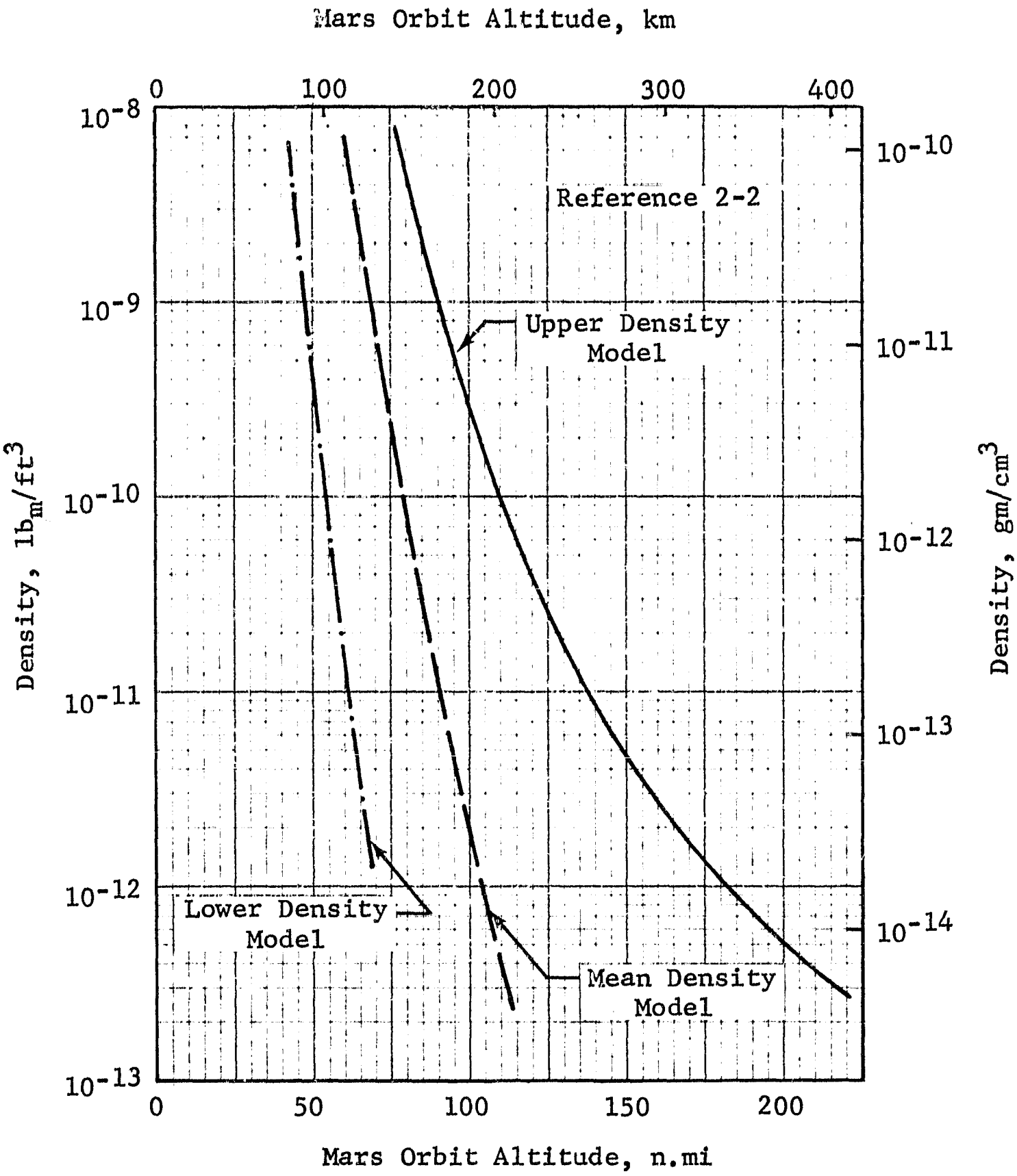

Figure 2.3-1 Martian Atmosphere Density Models

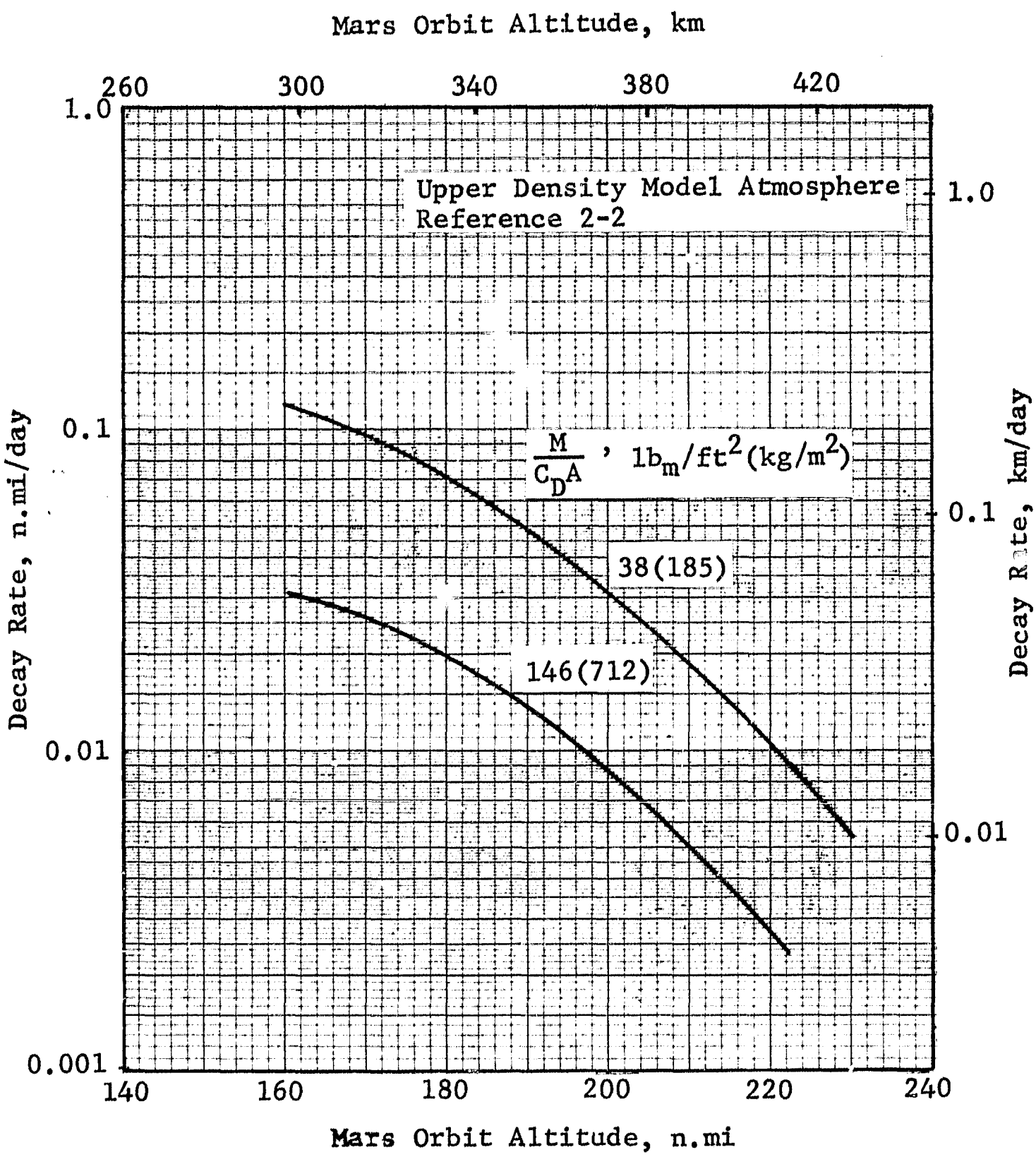

Figure 2.3-2 Variation of Orbit Decay Rates with Altitude

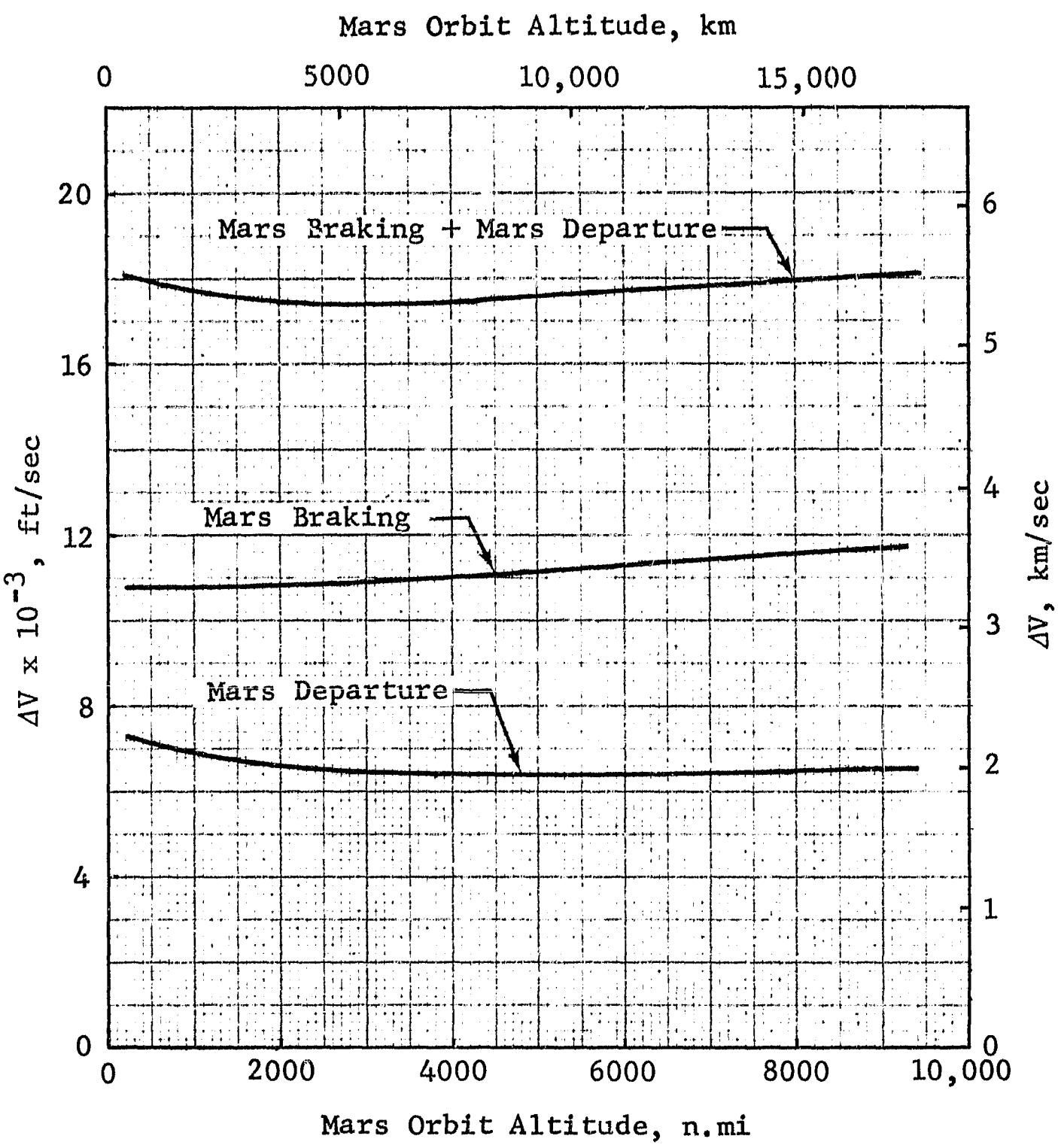

Figure 2.3-3 ΔV Requirements for Mars Braking and Departure vs Altitude

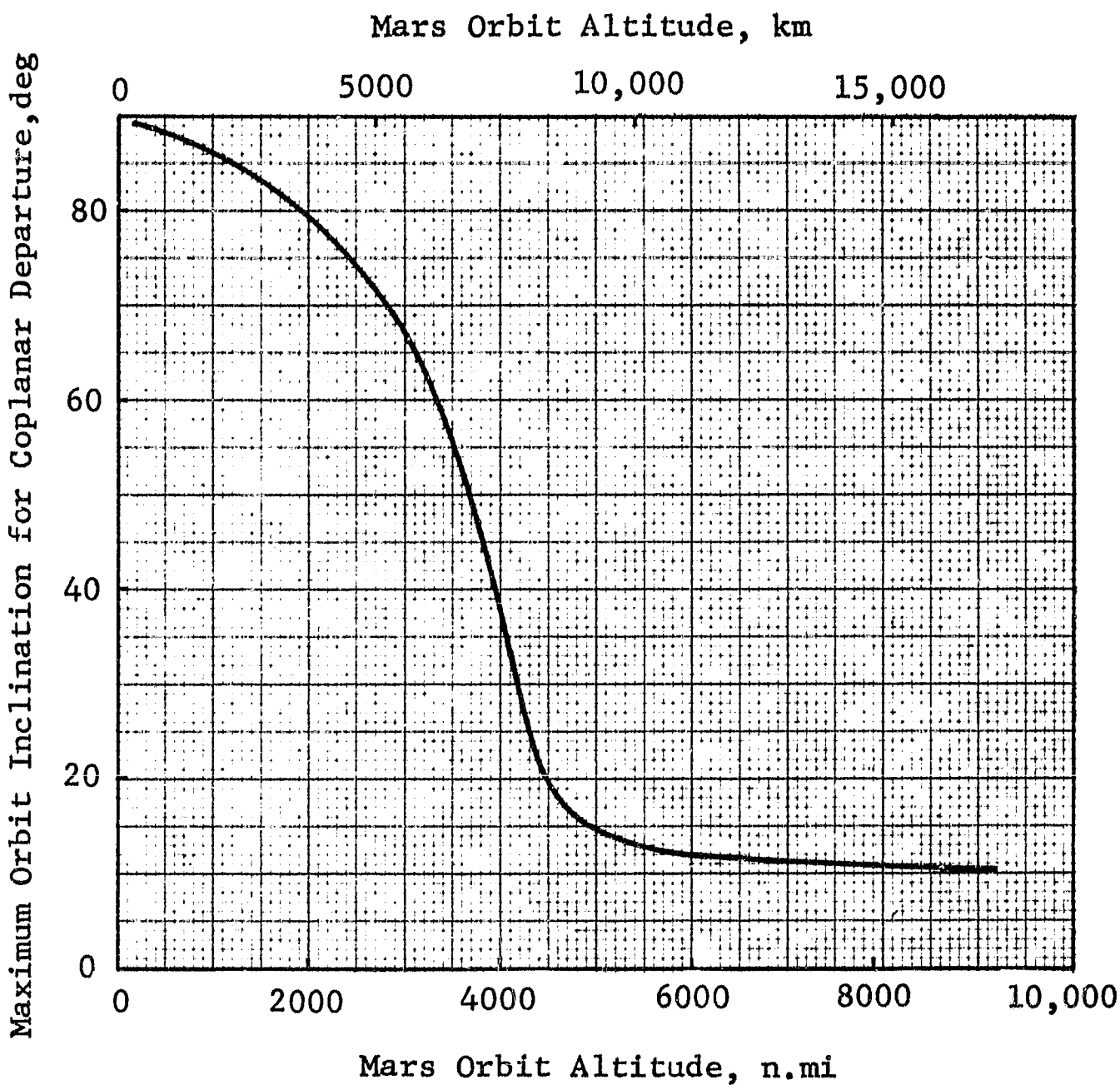

Figure 2.3-4 Variation of Maximum Orbit Inclination with Altitude

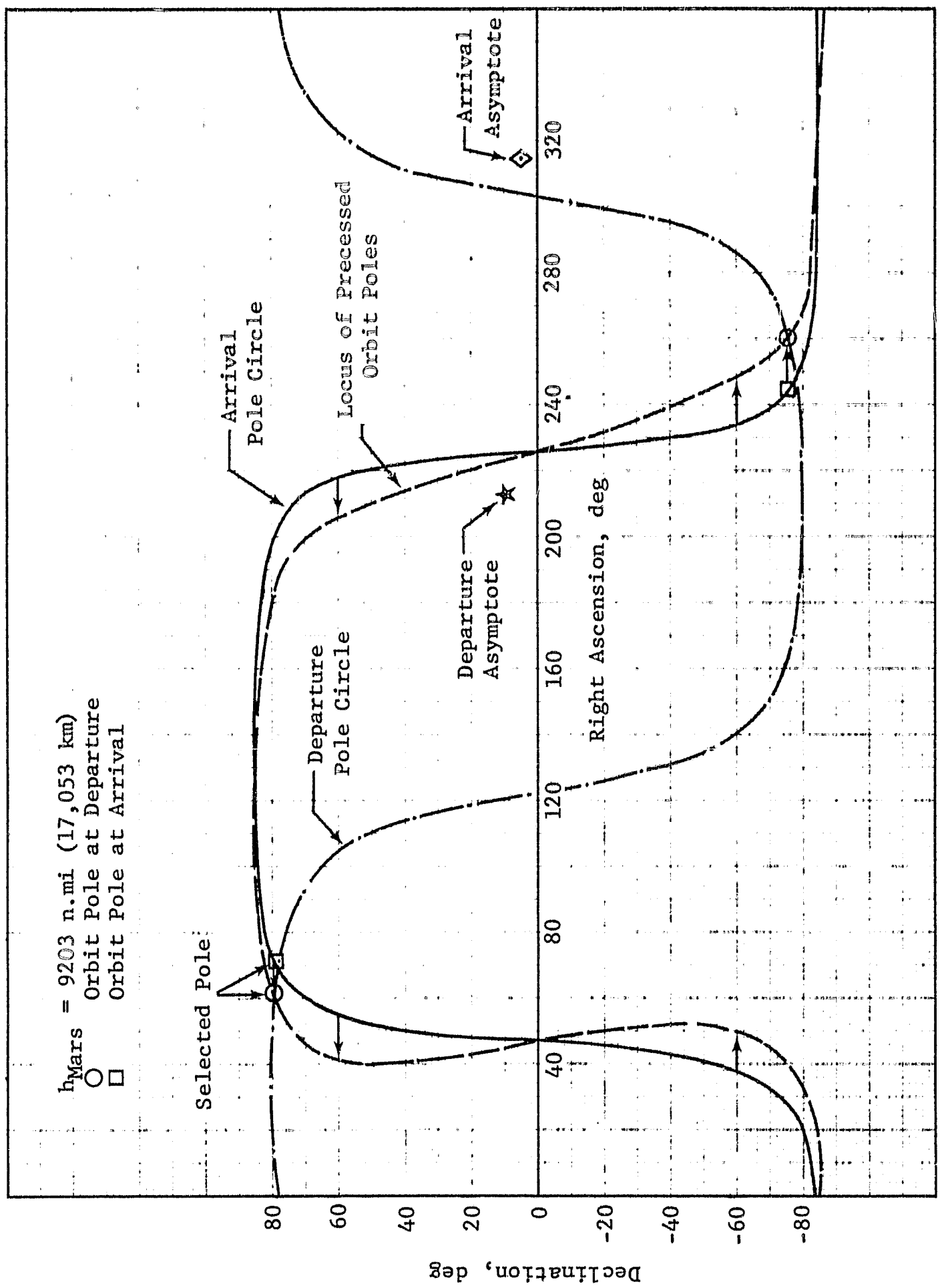

Figure 2.3-5 Mars Orbit Orientation Analysis: h_{Mars} = 9203 n.mi

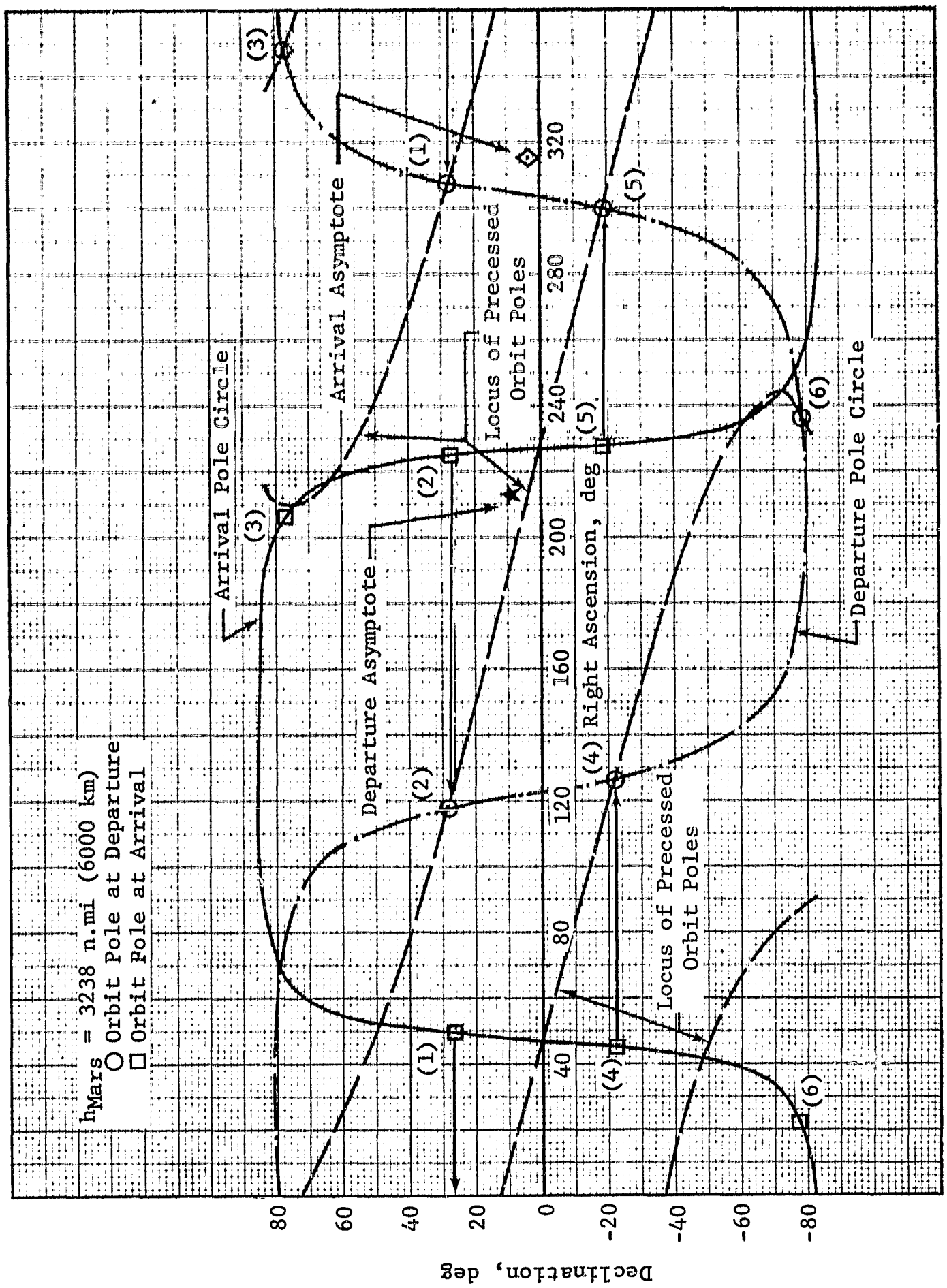

Figure 2.3-6 Mars Orbit Orientation Analysis: h_{Mars} = 3238 n.mi

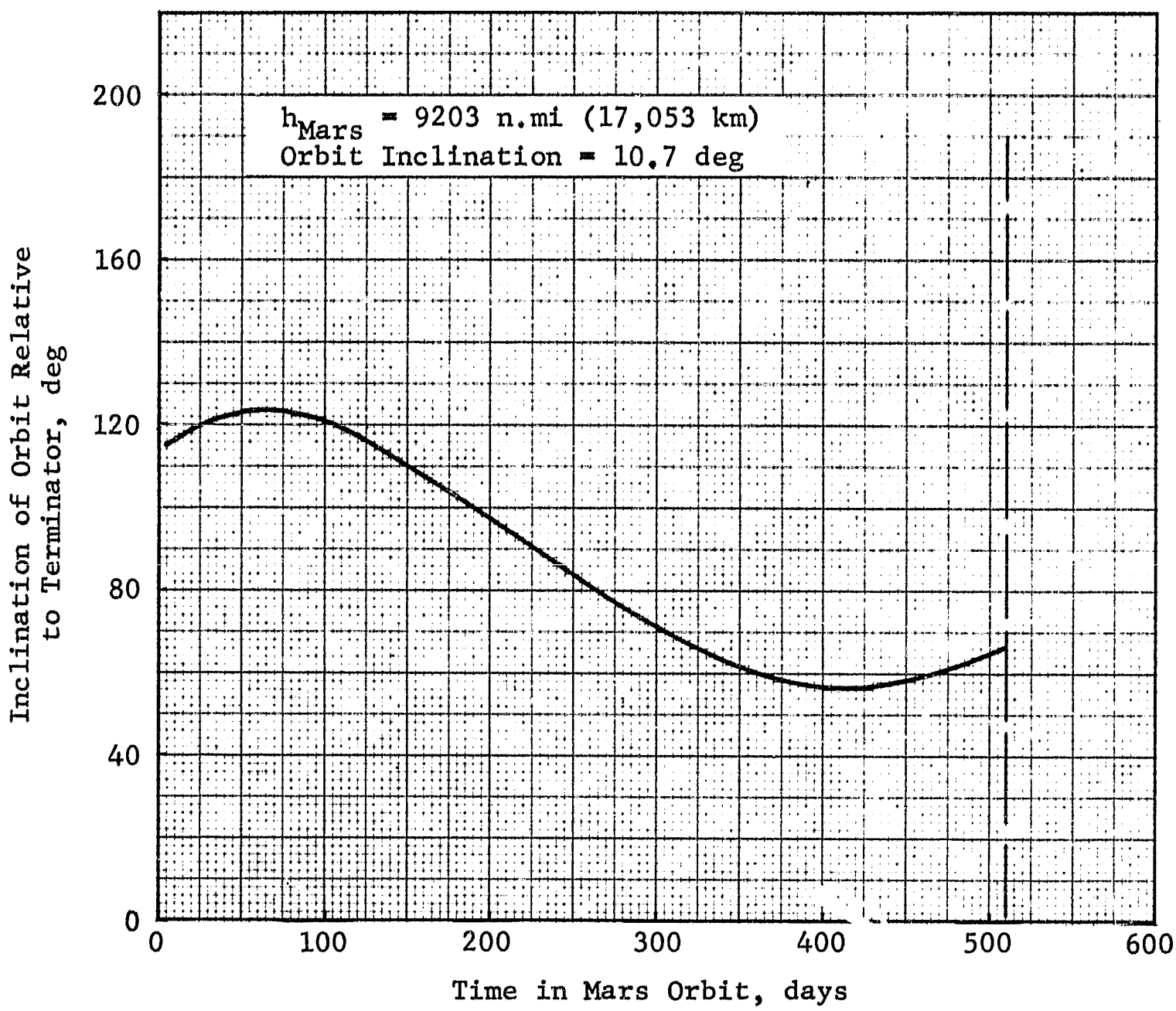

Figure 2.3-7 Mars Orbit Orientation History: h_{Mars} = 9203 n.mi

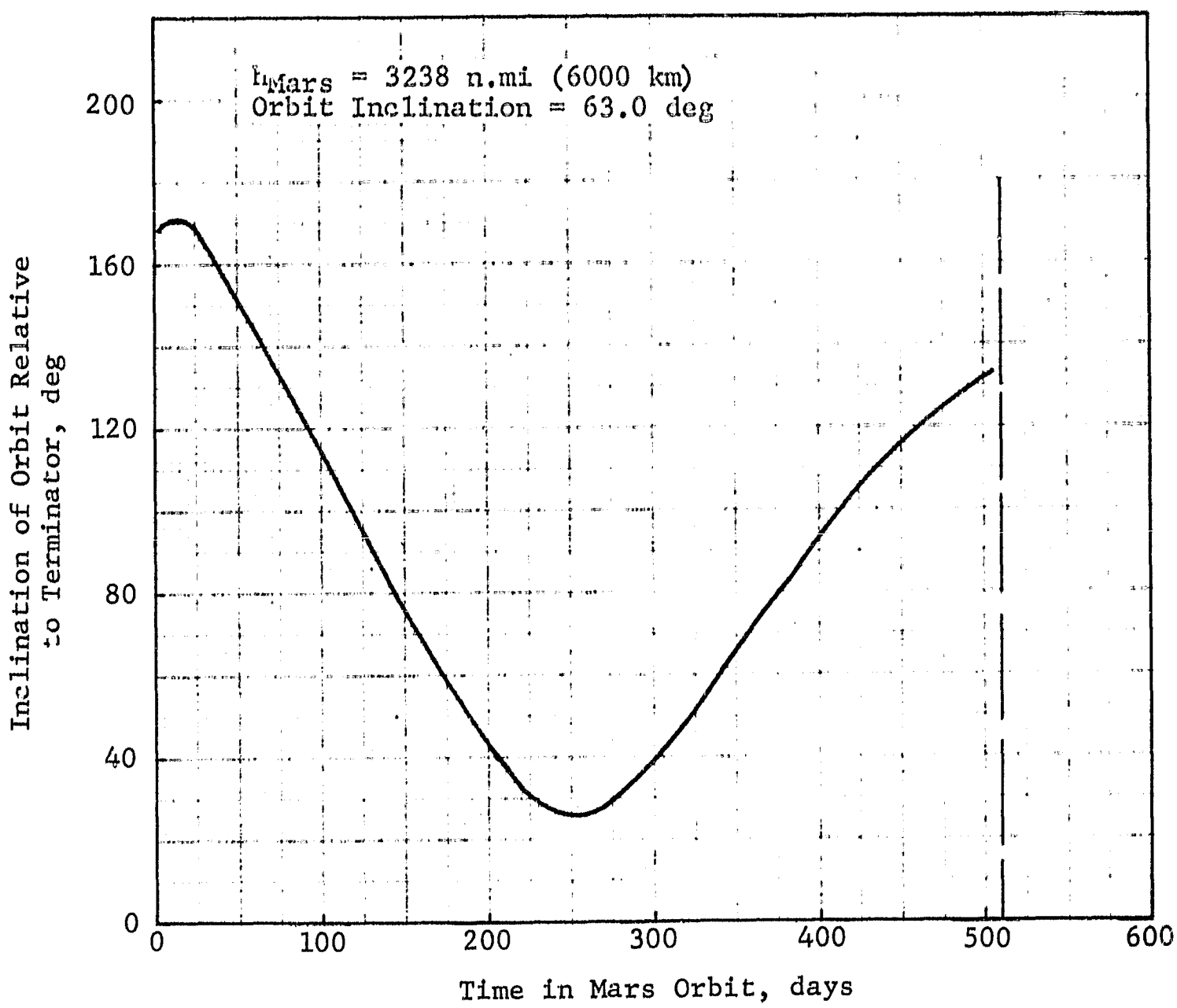

Figure 2.3-8 Mars Orbit Orientation History: h_{Mars} = 3238 n.mi

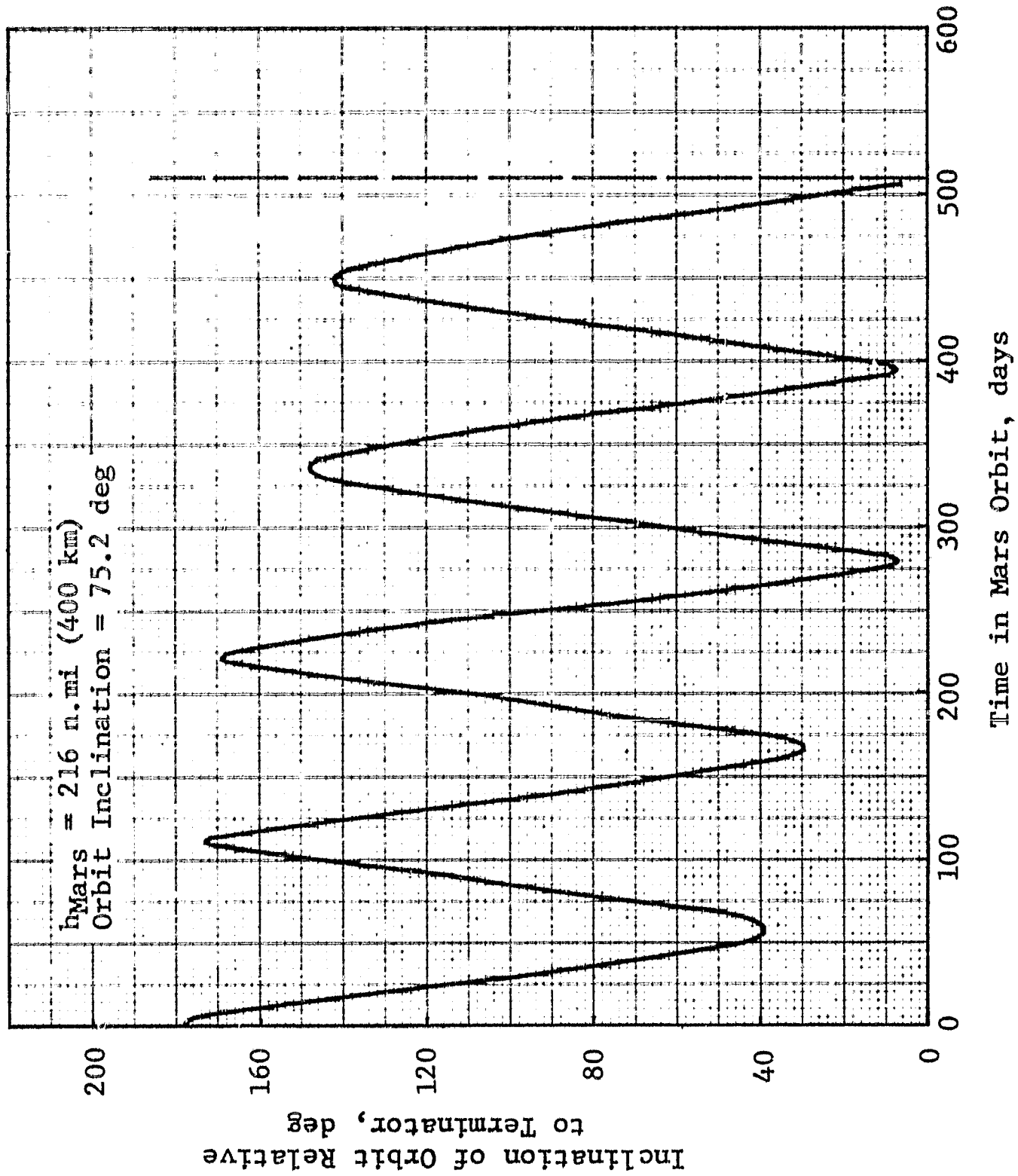

Figure 2.3-9 Mars Orbit Orientation History: h_{Mars} = 216 n.mi

PRECEDING PAGE BLANK NOT FILMED

SECTION 3

VEHICLE DEFINITION

The conjunction-class manned Mars vehicle which serves as the reference vehicle for this study is based on the modular concept. Each stage of the vehicle is built up from basic propellant and propulsion modules with the number of modules determined by the propellant requirements for the particular stage and the payload capability of the uprated Saturn V launch vehicle. The propellant tank size is dependent upon the variables investigated in this study and is not constant between the stages of the vehicle. However, all modules of a particular stage are identical with respect to tank size.

The basic propulsion module is described in Subsection 3.1 and the Mars vehicle configuration is discussed in Subsection 3.2. Analysis of the Mars Excursion Module and the evaluation of the MEM mass variation with Mars orbit altitude is presented in Subsection 3.3.

3.1 NUCLEAR PROPULSION MODULE

The nuclear propulsion module is based on the design concept of a load-carrying shell with a pressure-stabilized, membrane tank hung within the shell, as shown in Figure 3.1-1 (Ref. 3-1). During ascent to the assembly orbit, the outer shell carries the loads. However, once the vehicle is assembled and the ascent shells jettisoned, the tank wall becomes a part of the load-carrying structure.

The 32-ft (9.75 m) diameter propellant tank has a variable cylindrical length to accommodate propellant loadings for a wide variety of missions. By varying the number of barrel sections, the module can be tailored to the particular mission propellant requirements. The tank material is 2021-T81 aluminum alloy and the end closures are elliptical with an eccentricity of 0.7074. The tank is supported within the ascent shell by a support cone. This support cone carries the tank and engine in tension during Earth launch and transmits the thrust loads to the forward thrust structure during engine operation. The aft skirt carries some stabilizing loads during Earth launch, but is primarily designed

to transmit thrust loads from lower stages. Both the support cone and the aft skirt are of sheet-stringer design with titanium used extensively to reduce the penetration heat transfer. The forward thrust structure is connected to the tank support cone and transmits thrust loads to higher stages through the docking structure. It is fabricated of aluminum honeycomb and furnishes meteoroid protection for the tank head. The orbital assembly interstage is connected to the aft skirt and transmits thrust loads from lower stages; it is an aluminum honeycomb structure. The interstage also furnishes meteoroid protection to the tank head and engine and supports the docking cone.

Propulsion is furnished by the 5000 MW NERVA engine with a nominal thrust of 230,000 lb_f (1,023,000 N) and a specific impulse of 850 lb_f-sec/lb_m (8330 N-sec/kg). Total engine mass is 35,000 lb_m (15,900 kg) including nuclear shielding. Propellant modules are similar to propulsion modules with the exception of the engine.

Meteoroid protection is provided during some portion of the mission by the interplanetary meteoroid shield, the ascent shell, the tank wall, the orbital assembly interstage and docking cone, and the forward thrust structure. The tank wall furnishes the necessary protection for a one-hour period between the jettisoning of the meteoroid shield and engine operation. Protection during the interplanetary portion of the mission is furnished by the combination of the interplanetary meteoroid shield and the tank wall. This shield is a three-sheet aluminum structure with the spaces between the sheets filled with low-density foam. During Earth orbit, the additional meteoroid protection requirements are met by the ascent shell, in combination with the meteoroid shield and the tank wall.

Thermal protection of the liquid-hydrogen propellant is provided by the multilayer insulation which is attached to the tank wall. Although jettisoning of a portion of the insulation with the meteoroid shield is a feasible concept, this technique was not considered in this study. Determination of the optimum insulation thickness was accomplished on the basis of the entire insulation system remaining with the tank.

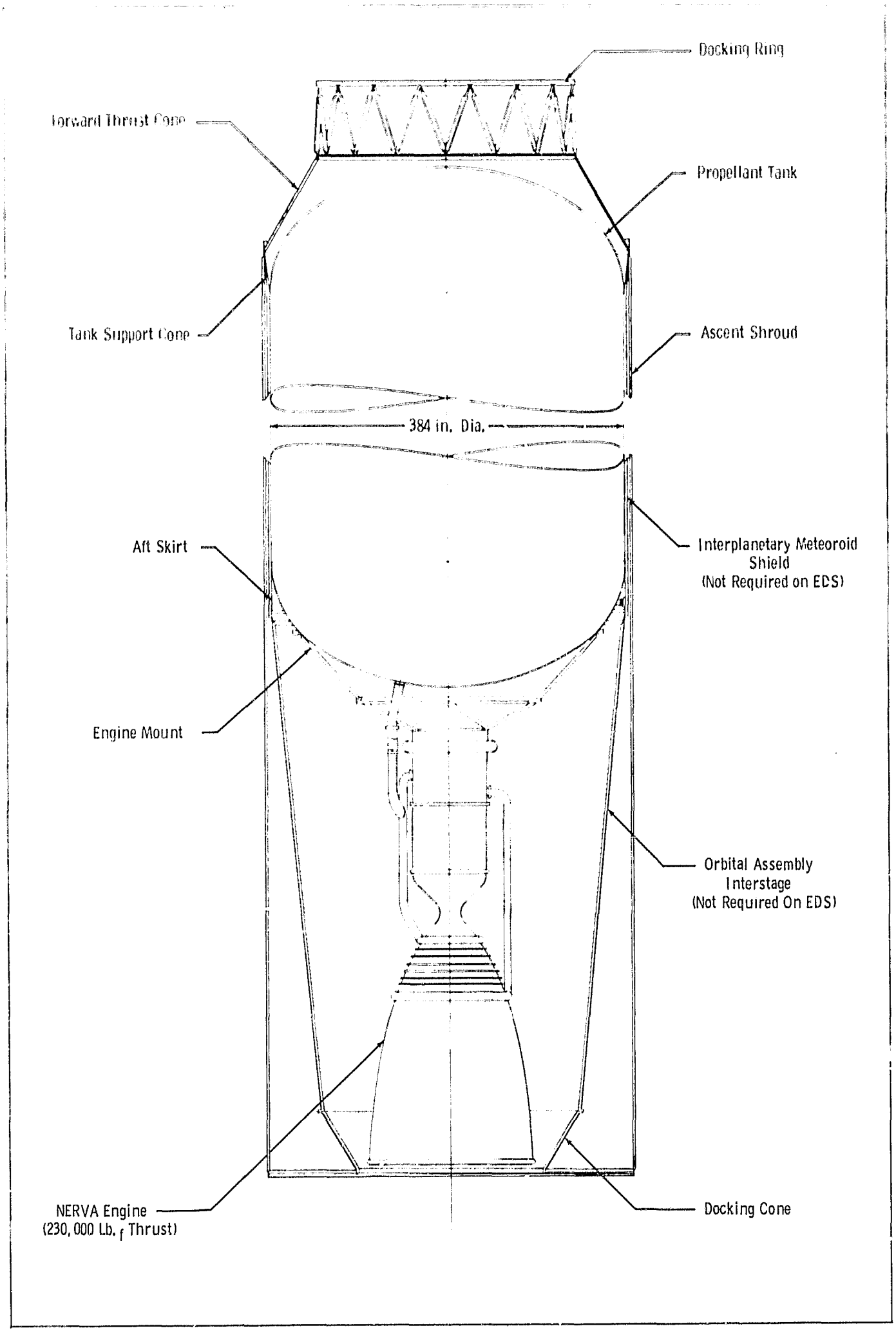

Figure 3.1-1 Nuclear Propulsion Module

3.2 CONJUNCTION-CLASS MARS VEHICLE

With the modules described in the previous subsection, a vehicle can be assembled for a wide variety of missions. The conjunction-class Mars stopover mission to which this study is referenced requires a three-stage vehicle to accomplish the Earth departure, Mars braking, and Mars departure maneuvers. The selected vehicle configuration is shown in Figure 3.2-1.

The Mars vehicle is made up from five propulsion modules, two propellant modules, and the spacecraft which includes the Mission Module, the Mars Excursion Module, and the Earth Entry Vehicle. Earth Departure Stage includes four modules with a propellant module stacked above the central propulsion module. The modules are arranged in an in-line configuration. This arrangement allows more similarity between modules, permits the thrust loads to be easily transmitted to the other stages, and is compatible with the concept of jettisoning the ascent shells just prior to Earth departure. Four modules were required to maintain a constant configuration over the range of variables investigated during the study. Preliminary analysis of the propellant loadings indicated that three modules would not be sufficient, in a number of cases, without the module mass exceeding the launch capability of the uprated Saturn V launch vehicle. For purposes of this study, this launch capability is assumed to be 330,000 lb_m (150,000 kg) in a 262 n.mi (485 km) assembly orbit.

The Mars Braking Stage is composed of two modules, a propellant module and a propulsion module. These modules are stacked above the propellant module of the Earth Departure Stage. The third or Mars Departure Stage is the smallest of the three stages and consists of a single propulsion module.

Assembly of the Mars vehicle in the 262 n.mi (485 km) assembly orbit occurs in the following sequence. First, the central propulsion module of the Earth Departure Stage is launched into orbit. The outer modules are then docked sequentially with the central module at their forward ends and swung into position. The Earth Departure Stage is completed with the docking of the propellant module. The two modules of the Mars Braking Stage are then assembled together and the combination docked to the Earth Departure Stage. The

vehicle is completed with the docking of the Mars Departure Stage and the modules comprising the vehicle payload.

The mission time history in this study begins with the assembly period in Earth orbit. For simplicity, it is assumed that all modules of the Earth Departure Stage are in Earth orbit for the entire staytime. The modules of the Braking Stage are in orbit for two-thirds of the total staytime and the single module of the Mars Departure Stage for one-third of the staytime. Shortly before engine ignition for departure from Earth orbit, the ascent shells, which have been used as meteoroid protection during the orbit period, are jettisoned. After the departure from Earth orbit, the first stage is separated and the Mars transfer solar shield, if used, is deployed at the aft end of the vehicle, as shown in Figure 3.2-2. Initial guidance corrections must be made before the shield is deployed, however, since the shield structure cannot withstand the guidance-correction loads. The solar shield must be jettisoned before the final guidance correction period, which occurs prior to entry into Mars orbit. Prior to the firing of the Mars Braking Stage engine, the foam-filled meteoroid bumpers of both modules and the orbital assembly interstage are jettisoned from the stage.

Once the Mars parking orbit is established, the Mars orbit solar shield may be deployed and the operations related to exploration of the planet surface commenced. The shielded vehicle configuration in Mars orbit is shown in Figure 3.2-3. The Mars Departure Stage remains in orbit while the Excursion Module transports the landing party and support equipment to the planet's surface. Near the end of the 510-day Mars orbit staytime, the ascent stage of the Excursion Module returns the landing party to the orbiting stage. Prior to engine firing, the meteoroid shield and the orbital assembly interstage are jettisoned. The Excursion Module is left at Mars since its function has been fulfilled. The return leg of the mission is completed with atmospheric braking at Earth, so that no hydrogen tanks are necessary for the return phase of the mission. Thus, the return leg of the mission does not enter into the analyses conducted during this study.

Optimization of the stage propellant storage system was accomplished on a single stage basis. To obtain the vehicle IMIEO, it was necessary to define a nominal vehicle and determine the mass fractions for the non-jettisoned propellant storage components, the boiloff during each mission phase, and the meteoroid protection, for each stage. These mass fractions were used to define the propellant storage systems of the vehicle stages other than the one being optimized. The nominal stages were defined to correspond to stages having highly efficient propellant storage systems and this has some effect on the results of the analysis. Had the nominal stages been defined with less effective propellant storage systems, these stages would have been heavier and the effects of the parameters would have been magnified. The nominal mass fractions are presented in Table 3.2-1.

For purposes of comparison, some of the results of the analysis have been referenced to a "zero-mass-fraction" vehicle. Actually, two vehicles of this type are referred to in this report depending upon the vehicle being compared. In the optimization analyses, only one stage of the vehicle is investigated while the remaining two stages are defined with nominal mass fractions. The corresponding "zero-mass-fraction" vehicle used for comparison has a propellant storage system mass fraction of zero <u>only</u> for the stage being studied. The remaining stages are defined with the same nominal mass fractions used in the optimization analysis. This allows the isolation of the effects of the basic parameters and systems to the particular stage and ensures a proper determination of the effect on the vehicle IMIEO.

The second "zero-mass-fraction" vehicle is referred to in Subsection 4.1 of Volume 1. In that subsection, the effects of the study variables are analyzed with all three stages of the vehicle defined in terms of the optimum propellant storage component mass fractions. Thus, for comparison, all three stages of the "zero-mass-fraction" vehicle have propellant storage system mass fractions of zero.

Table 3.2-1 NOMINAL STAGE MASS FRACTIONS

Mars Orbit Altitude	Stage	Non-Jettisoned Propellant Storage System Mass Fraction	Boiloff Mass Fractions			Meteoroid Protection Mass Fraction
			Earth Orbit	Mars Transfer	Mars Orbit	
216 n.mi (400 km)	Earth Departure	0.10	0.02	--	--	0.0
	Mars Braking	0.10	0.0	0.04	--	0.0170
	Mars Departure	0.11	0.0	0.04	0.19	0.0202
3238 n.mi (6000 km)	Earth Departure	0.10	0.02	--	--	0.0
	Mars Braking	0.10	0.0	0.04	--	0.0181
	Mars Departure	0.11	0.0	0.05	0.16	0.0174
9203 n.mi (17,053 km)	Earth Departure	0.10	0.02	--	--	0.0
	Mars Braking	0.10	0.0	0.03	--	0.0188
	Mars Departure	0.11	0.0	0.06	0.14	0.0163

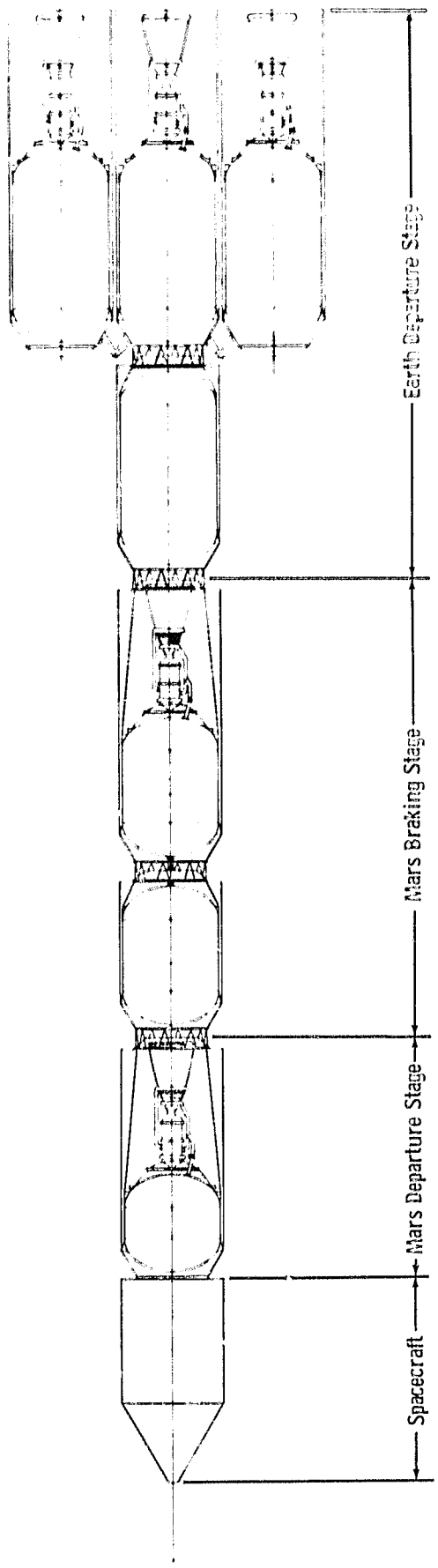

Figure 3.2-1 Conjunction-Class Mars Vehicle

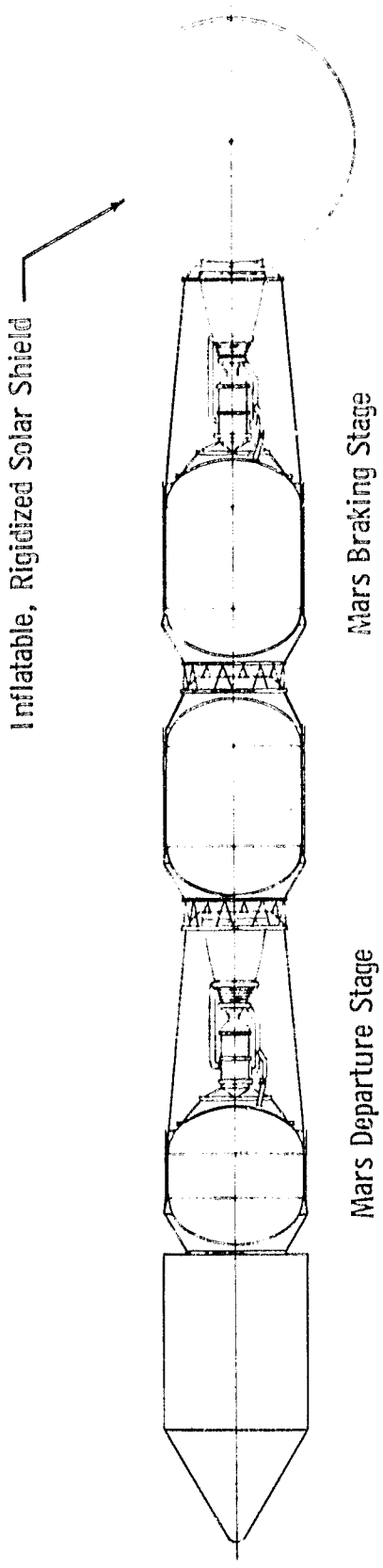

Figure 3.2-2 Mars Transfer Solar Shield-Vehicle Configuration

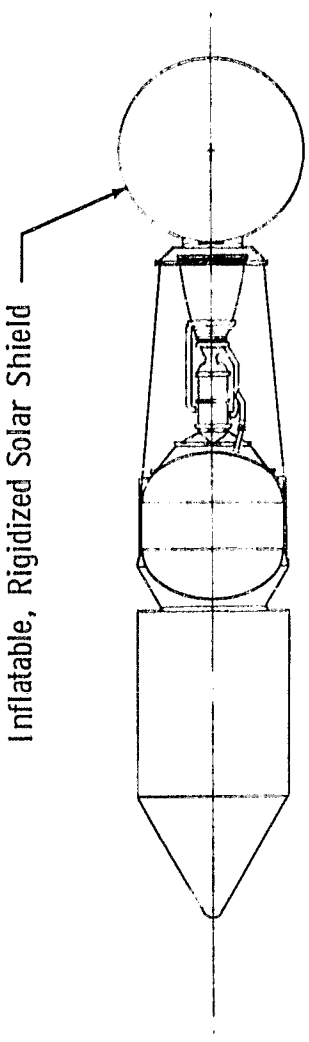

Figure 3.2-3 Mars Orbit Solar Shield-Vehicle Configuration

3.3 MARS EXCURSION MODULE ANALYSIS

Trajectory/vehicle analysis of the Mars Excursion Module (MEM) was aimed at evaluating the variation of MEM mass with circular-orbit altitude. The main effort was devoted to determining the mass variation with a consistent set of assumptions and no attempt was made to optimize mass, the propulsion system, or the energy requirements. The analysis was based on the MEM defined in Reference 3-2, which is designed for a 6-man crew and a nominal staytime of 500 days. The most important deviation from the reference MEM was the choice of propellants. Storable propellants (specific impulse = 360 lb_f sec/lb_m (3530 N sec/kg) were assumed rather than cryogenic propellants because of the long staytime on the planet.

The trajectory for the ascent vehicle is a direct ascent to an altitude of 100 n.mi (185 km) followed by a Hohmann transfer to the selected parking orbit. To ascend to 100 n.mi (185 km), the ΔV is 15,000 ft/sec (4.57 km/sec), with allowances for drag and gravity losses included. The ΔV for the Hohmann transfer was multiplied by a factor of 1.05 to account for gravity losses, plane change requirements, and terminal rendezvous requirements.

A two-stage ascent vehicle was defined. The first stage is used for the ascent to 100 n.mi (185 km) and the second stage is used for the transfer to the parking orbit. A two-stage vehicle rather than a one-stage vehicle was defined to reduce the ascent vehicle mass resulting from the relatively high energy requirements for transfer to the synchronous altitude. Payload of the ascent vehicle is 11,310 lb_m (5130 kg) and includes the crew and associated equipment; control, tracking, and computer equipment for piloting the stage; and the scientific payload and samples brought from the surface. The structural mass of each stage was based on a propellant mass fraction (propellant mass divided by the sum of propellant mass and structural mass) of 0.90. Engine mass, tank mass, propellant subsystems mass, etc., are included in the structural mass.

The sequence of events for descent consists of a transfer from the parking orbit to an entry altitude of 54 n.mi (100 km), lifting entry, propulsive braking, hover, translation and landing. Parachute braking was not considered

because the data given in Reference 3-3 indicate that it may not be feasible. Figure 3.3-1 presents the variation of the entry velocity and the deorbit ΔV with entry flight-path angle for the three selected altitudes. The deorbit ΔV is tangential (directed 180 degrees to the velocity vector). Note that the variation of the entry velocity and deorbit ΔV with entry angle is small for the higher altitudes. The entry angles were selected to be near a skipout boundary (approximately the minimum angle where the altitude is always decreasing for ballistic entry into the lower-density model atmosphere of Ref. 3-3). A fixed ΔV allowance for propulsive braking, translation, and hovering was used because the primary effect of orbit altitude on ΔV requirements should be reflected in the ascent Hohmann transfer ΔV and the descent deorbit ΔV. Propulsive braking, translation, and hovering requirements are primarily dependent upon entry and final touchdown techniques, e.g., L/D modulation, specified distance (translation), and time (hover), rather than on orbit altitude. The required propulsive braking ΔV is 1640 ft/sec (0.5 km/sec)(Ref. 3-3) and the ΔV allowance for hover and translation is 1300 ft/sec (0.396 km/sec)(Ref. 3-2).

A single-stage descent vehicle was defined with the payload consisting of the surface payload and the ascent vehicle. Included in the surface payload of 62,660 lb_m (28,420 kg) are two roving vehicles, life support equipment and supplies, experimental equipment, power supply, and other items to maintain a base on the surface. In addition to the normal structure based on a propellant mass fraction of 0.85, a landing gear and heat shield were included. The mass of the heat shield was defined as 3.5% of the gross MEM mass and part of the heat shield was assumed to be ablated and/or jettisoned prior to propulsive braking. The mass of the landing gear was defined as 1% of the landed mass.

On the basis of the foregoing vehicle/trajectory definitions, the variation of MEM mass with Mars orbit altitude was determined. The gross mass of the MEM is presented as a function of altitude in Figure 3.3-2. A detailed mass breakdown of the MEM for each of the selected altitudes is presented in Table 3.3-1. The data in Table 3.3-1 indicate that the increase in MEM mass with increasing altitude results primarily from the larger propellant requirements associated with the higher ΔV requirements for the transfer performed by the second ascent stage and for descent-deorbit.

Table 3.3-1 MARS EXCURSION MODULE MASS BUILDUP

	Mass at Indicated Mars Orbit Altitude lb_m(kg)		
	216 n.mi (400 km)	3238 n.mi (6000 km)	9203 n.mi (17,053 km)
Ascent Payload	11310 (5130)	11310 (5130)	11310 (5130)
Second Ascent Stage Structure	40 (18)	600 (272)	905 (411)
Second Ascent Stage Propellant	340 (154)	5400 (2449)	8130 (3688)
Mass at Second Stage Ignition	11690 (5302)	17310 (7852)	20345 (9228)
First Ascent Stage Structure	4875 (2211)	7220 (3275)	8490 (3851)
First Ascent Stage Propellant	43935 (19929)	65065 (29513)	76465 (34684)
Gross Mass at Liftoff	60500 (27443)	89595 (40640)	105300 (47764)
Landing Gear	1360 (617)	1755 (796)	1955 (887)
Heat Shield	4590 (2082)	6805 (3086)	7780 (3529)
Surface Payload	62660 (28422)	62660 (28422)	62660 (28422)
Descent Stage Structure	7895 (3581)	16305 (7396)	19570 (8877)
Total Landed Mass	137005 (62145)	177120 (80341)	197265 (89479)
Propellant (Propulsive Braking, Hover, and Translation)	39615 (17969)	51215 (23231)	57040 (25873)
Mass at Second Ignition	176620 (80114)	228335 (103572)	254305 (115352)
Heat Shield and Nose Cap	1835 (832)	2720 (1234)	3110 (1411)
Propellant (Deorbit)	5120 (2322)	41160 (18670)	53850 (24426)
Gross MEM Mass	183575 (83269)	272215 (123476)	311265 (141189)

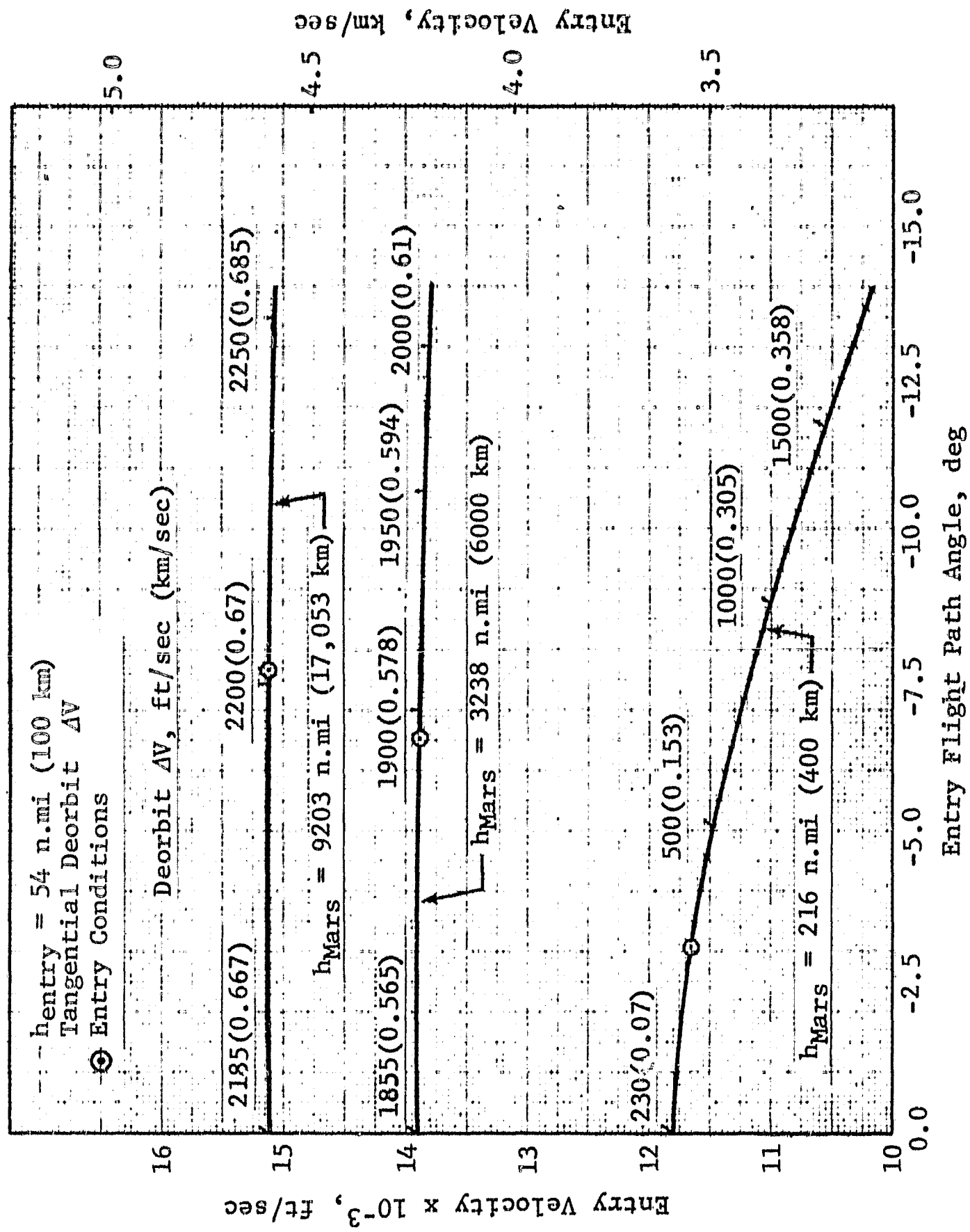

Figure 3.3-1 MEM Deorbit Entry Conditions

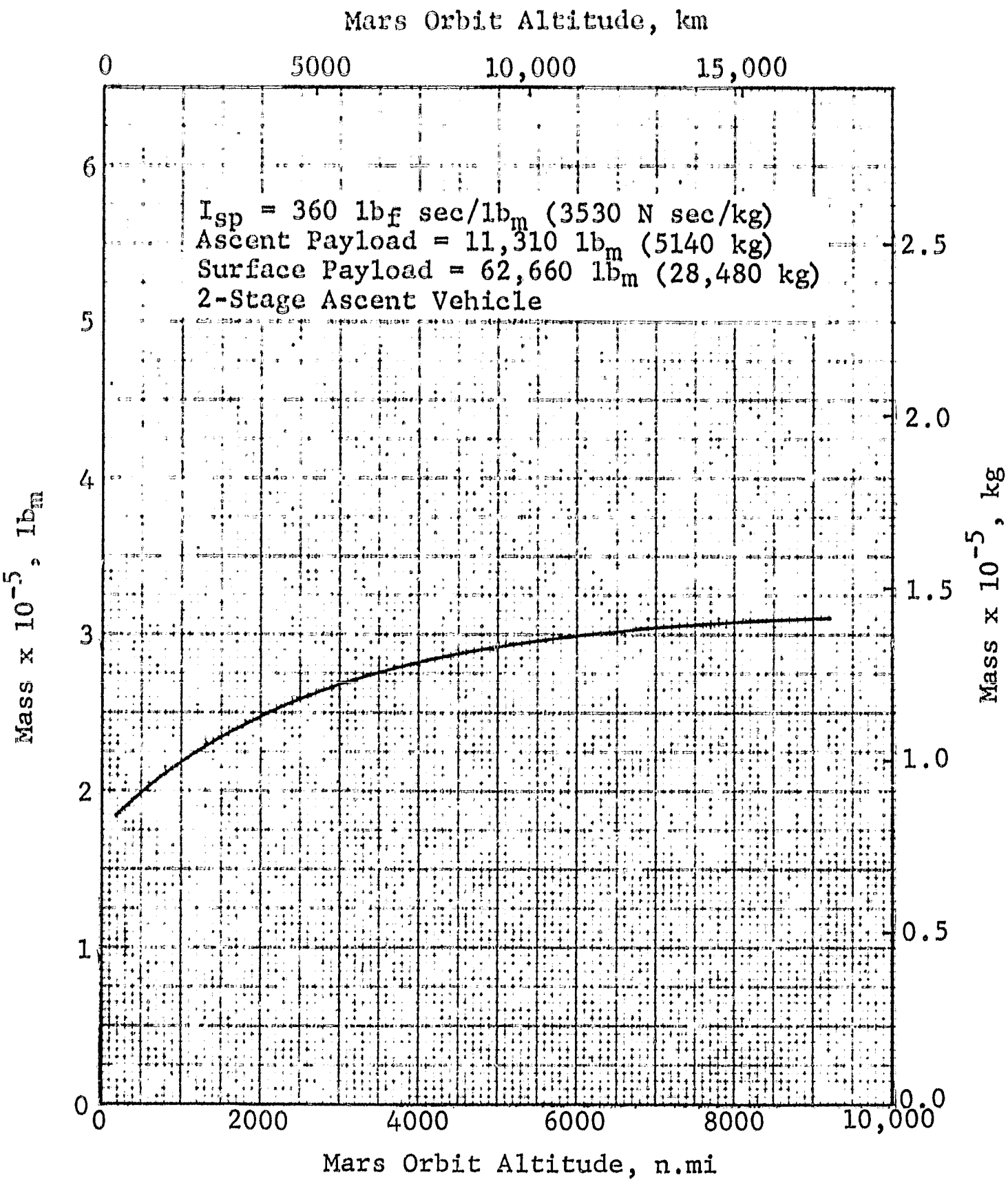

Figure 3.3-2 Variation of MEM Mass with Altitude

3.4 MASS BUILDUP DATA

To obtain a relatively complete mass-buildup of the vehicle, mass values were assigned to components that are not affected by the variables investigated in this study. These mass values are presented in Table 3.4-1 and generally follow the data of Reference 3-1. Where the component mass is peculiar to a single stage of the vehicle, this fact is noted.

Table 3.4-1 MISCELLANEOUS COMPONENT MASSES

Component	Mass, lb_m(kg)
Payload adapter (Mars Departure Stage)	2300 (1040)
Female docking structure	2840 (1290)
Orbital-assembly interstage	6250 (2830)
Docking cone	1044 (475)
Propulsion-to-propellant-module interstage (Mars Braking Stage)	2100 (950)
Fuel interconnect (Mars Braking Stage)	220 (100)
Propulsion-to-propellant-module interstage (Earth Departure Stage)	2100 (950)
Fuel interconnect (Earth Departure Stage	1000 (455)
Clustering structure (Earth Departure Stage)	4585 (2080)
Electronics, telemetry, etc.	3800 (1720)
Engine disposal system (propulsion module)	1500 (680)

PRECEDING PAGE BLANK NOT FILMED.

SECTION 4

THERMAL ANALYSIS

Evaluation of the propellant heat transfer is an important part of the thermal protection system optimization. In this section, the methods used to compute this heat transfer are described. A necessary first step in any thermal analysis is the definition of the thermal model. The model selected for this study is discussed in Subsection 4.1 and is fairly general, permitting maximum potential for extension of the data to other propellant tank configurations.

The Mars vehicle experiences three different thermal environments: Earth orbit, Mars transfer, and Mars orbit. Determination of the quantity of thermal radiation incident upon the vehicle during these mission phases is treated in Subsection 4.2.

In addition to heat transfer through the tank-wall insulation, structural components and piping penetrate through the insulation and provide ready paths for heat transfer to the propellant. This mode of heat transfer is discussed in Subsection 4.3.

4.1 THERMAL MODEL

The complexity of a thermal model is dependent to a great extent on the kind of thermal data that is desired and the desired accuracy. In this study the heat transfer to the propellant is the important quantity; no requirement exists for detailed temperature data. Therefore, a relatively simple thermal model was defined to evaluate the heat transfer in the optimization analyses.

In the actual module, circumferential conduction in the ascent shell, the meteoroid shield, and the multilayer insulation will tend to reduce circumferential temperature gradients. Therefore, in the thermal model, a uniform-temperature external surface was assumed. The resistance to heat transfer offered by the ascent shell and meteoroid shield have been neglected in this study. The only resistance considered is that due to a material of thermal conductivity, k, and density, ρ. This allows the data to be extended to other wall configurations by interpreting the conductivity and density as "effective" values for a composite wall structure.

The external surface receives solar radiation both directly and after reflection from the Earth or Mars, depending upon the mission phase. Thermal radiation emitted by these planets also is incident upon the surface. Energy leaves the surface by radiant emission to space and by a complex radiative-conductive process through the multilayer insulation to the propellant. Superimposed on, but independent of, the heat transfer through the insulation is the penetration heat transfer which is discussed in more detail in Subsection 4.3.

During all mission phases, the external surface of the module is assumed to be coated with the Lockheed Optical Solar Reflector thermal control coating. The properties of this coating are a solar absorptance of 0.05 and an emittance of 0.80, with an area density of 0.115 lb_m/ft^2 (0.560 kg/m^2) (Reference 4-1).

4.2 THERMAL ENVIRONMENT EVALUATION

Evaluation of the thermal environment experienced by the Mars vehicle is separated into the three chronological divisions corresponding to the separate mission phases of Earth orbit, Mars transfer, and Mars orbit. The data of Reference 4-2 has been used to evaluate the two orbital environments.

4.2.1 Earth Orbit

The Earth orbit altitude of 262 n.mi (485 km) is a commonly assumed altitude for assembly of interplanetary vehicles. For this altitude, a comparison was made of the adiabatic wall temperature, averaged over the orbit, for three combinations of vehicle orientation and orbit inclination. The results, shown in Table 4.2-1, are based on a cylindrical geometry with the surface radiative properties corresponding to the Optical Solar Reflector surface.

Table 4.2-1 COMPARISON OF EARTH-ORBIT ADIABATIC WALL TEMPERATURES

Orbit	Vehicle Orientation	Temperature $^{o}R(^{o}K)$
Terminator	Solar	347(193)
Terminator	Broadside	361(201)
Noon	Solar	340(189)

Since the maximum temperature difference is only 6.2%, the terminator orbit with broadside orientation was selected as the basis for Earth orbit heat transfer.

In the optimization analysis computer program, the input requires the absorbed heat flux. For Earth orbit this absorbed heat flux, averaged over the vehicle surface, is 25.7 Btu/hr-ft^2 (80.7 W/m^2). This corresponds to an adiabatic wall temperature of 370°R (205°K). This value is based on a cylindrical surface and is slightly higher than the value in Table 4.2-1 which is based on a cylinder, including the ends.

4.2.2 Mars Transfer

During Mars transfer, the unshielded vehicle is oriented broadside to the sun for the entire 210-day outbound leg. Since the solar distance increases from 1.0 to 1.5 AU (see Figure 2.1-2), the absorbed heat flux is not constant but varies from 7.21 to 3.60 Btu/hr-ft^2 (22.7 to 11.4 W/m^2). This heat flux is averaged over the entire cylindrical surface.

For the shielded case, it is assumed that the solar shield reduces the energy incident upon the vehicle to a negligible value. The heat transfer during the two one-hour guidance correction periods at the beginning and end of the outbound leg is considered however. The first period occurs before the shield is deployed and the second occurs after the shield is jettisoned. During these periods, the vehicle has a broadside orientation with respect to the sun and the absorbed heat flux is 5.4 Btu/hr-ft^2 (17.0 W/m^2). This heat flux corresponds to an adiabatic wall temperature of 250°R (139°K).

4.2.3 Mars Orbit

Three values of the Mars orbit altitude were examined: 216 n.mi (400 km), 3238 n.mi (6000 km), and 9203 n.mi (17,053 km). The basis for selection of these orbits, as well as the orbit geometries was discussed in Section 2. Of interest from a thermal environment standpoint is the inclination of the orbit with respect to the terminator. Figures 2.3-7, 2.3-8 and 2.3-9 show the time histories of the inclination to the terminator for each of the orbit altitudes. From these time histories, the average inclination to the terminator was obtained by graphical integration. These average inclinations are presented in Table 4.2-2.

Table 4.2-2 AVERAGE INCLINATION TO TERMINATOR FOR MARS ORBIT

Altitude, n.mi (km)	Inclination	Average Inclination to Terminator
216 (400)	75.2°	50.0°
3238 (6000)	63.0°	52.7°
9203 (17,053)	10.7°	66.0°

Based on these average inclinations, the variations in the absorbed heat flux over the orbit were determined, using a solar constant of 196.9 Btu/hr-ft^2 (621.1 W/m^2), an integrated albedo of 0.15, and a planet thermal radiation rate of 40.48 Btu/hr-ft^2 (127.0 W/m^2). The unshielded vehicles were oriented along the velocity vector in all cases. For the shielded case, the longitudinal axis of the vehicle was oriented parallel to the solar vector with the solar shield deployed from the aft end of the vehicle (see Figure 3.2-3). From the time variation of the absorbed heat flux, the average was determined by graphical integration, for each of the altitudes. These average heat flux values are assumed constant over the entire 510-day Mars orbit period and are tabulated in Table 4.2-3.

Table 4.2-3 AVERAGE ABSORBED HEAT FLUX FOR MARS ORBIT

Altitude, n.mi (km)	Heat Flux, $\frac{\text{Btu}}{\text{hr-ft}^2}\left(\frac{\text{W}}{\text{m}^2}\right)$	
	Unshielded	Shielded
216 (400)	11.78 (37.16)	9.09 (28.68)
3238 (6000)	4.00 (12.62)	1.15 (3.63)
9203 (17,053)	2.58 (8.14)	0.21 (0.66)

4.3 PENETRATION HEAT TRANSFER

With any tank design, it is necessary to have structural members, piping, and attachments which penetrate the insulation and provide conduction paths for heat transfer.

In the preliminary analyses, the thermal conductance of the tank support cone and aft skirt were evaluated as 0.805 Btu/hr-^{o}R (0.424 W/^{o}K) and 0.197 Btu/hr-^{o}R (0.104 W/^{o}K), respectively. Conductances for the piping and engine support were taken from Reference 3-1. The total penetration thermal conductance thus obtained, 1.764 Btu/hr-^{o}R (0.930 W/^{o}K), was used for all tanks in the preliminary analysis.

For the final analysis, consideration was given to reasonable reductions in the penetrations, where possible. It was concluded that a reduction in the thickness of the upper tank support was possible where the propellant tank mass was less than that for which the support was designed, provided a reasonable minimum thickness was observed (0.025 in or 0.064 cm for both plate and stringers). The Earth Departure Stage was sufficiently massive that no reduction was possible, but it was possible to reduce the conductances of the upper tank supports on the Mars Departure and Mars Braking Stages by 33.6% and 12.5%, respectively. In addition, the weighted average of the conductances was taken where both propulsion and propellant modules make up the stage, so that the propellant modules were not unduly penalized for heat transfer through an engine support structure which does not exist. This approach led to reduced conductances in both the Earth Departure Stage and the Mars Braking Stage.

The penetration heat transfer conductances used in the final analysis are tabulated below:

Stage	Conductance, $\frac{\text{Btu}}{\text{hr-}^{o}\text{R}}$ $\left(\frac{\text{W}}{^{o}\text{K}}\right)$
Earth Departure	1.889 (0.996)
Mars Braking	1.773 (0.935)
Mars Departure	1.577 (0.832)

These conductances were used with the difference between the adiabatic wall temperature and the propellant temperature to determine the penetration heat transfer rate.

The effect of the solar shield on the penetration heat transfer is direct, in that the reduction in the adiabatic wall temperature which results from the use of the shield yields a reduction in the temperature drop across the penetration.

PRECEDING PAGE BLANK NOT FILMED

SECTION 5

STRUCTURAL ANALYSIS

Two of the major components of the module propellant storage system are the propellant tank and the meteoroid protection system. In this section, the methods of evaluating the masses of the tank and the interplanetary meteoroid shield are described.

5.1 TANK MASS EQUATION

The tank mass equation used in this study includes the mass of the tank and the related structural mass that is proportional to the basic tank mass.

The equation presented here is simplified for use in the parametric study since a detailed stress analysis of all the components of the tank assembly was outside the scope of this work. However, the mass values generated with the final equation are reasonably accurate when compared to values developed by detailed analysis.

The basic portion of the tank mass equation is derived from the membrane hoop and meridianal stresses associated with thin-wall pressure vessels and the imposed ullage and hydrostatic pressures. It is a summation of the mass requirements due to the meridianal stresses on the elliptical upper and lower tank closures and the hoop stresses on the cylindrical portion. This mass can be termed the "pressure mass" and written as

$$\text{Pressure mass} = \rho_t F_s \left[\left\{ \pi a^2 + \frac{\pi b^2}{2e} \ln \left(\frac{1+e}{1-e} \right) \right\} \left\{ \frac{a^2}{b\sigma} \left(P + \rho n \frac{\ell}{2} \right) \right\} + 2\pi a \left(\ell - 2b \right) \left\{ \frac{a}{\sigma} \left(P + \rho n \frac{\ell}{2} \right) \right\} \right] \qquad (5\text{-}1)$$

The tank mass and average wall thickness are determined from Equation 5-1 using the worst possible combination of pressure and acceleration. The highest acceleration

occurs during Earth launch while the highest pressure occurs at the time of engine ignition. This pressure includes a 5.0 psi (3.45 N/cm^2) increment to simulate nuclear heating and satisfy the NPSP requirements of the pump. A minimum tank design pressure of 19.7 psia (13.6 N/cm^2) was used throughout the study. This pressure corresponds directly to the 14.7 psia (10.1 N/cm^2) vent pressure when the increment mentioned above is included. For the nonvent mode, the final pressure is a function of the final specific internal energy of the propellant. Thus, the pressure can exceed the minimum value resulting in a heavier tank.

The complete tank mass equation including related structural mass is obtained by applying a contingency factor, F_c, to Equation 5-1. This accounts for the mass of the tank components and related structure that are not included in the pressure requirements. Thus, the final tank-mass equation with contingency factor and safety factor, F_s, is

$$M_t = F_c F_s \rho_t \left[\left\{ \pi a^2 + \frac{\pi b^2}{2e} \ln\left(\frac{1+e}{1-e}\right) \right\} \left\{ \frac{a^2}{b\sigma} \left(P + \rho n \frac{\ell}{2} \right) \right\} + 2\pi a (\ell - 2b) \left\{ \frac{a}{\sigma} \left(P + \rho n \frac{\ell}{2} \right) \right\} \right] \qquad (5\text{-}2)$$

A contingency factor of 1.75 was used throughout the study based on the results of a survey of existing hardware and previous detailed studies. The items included in the contingency factor are listed below as a percentage of the basic pressure mass.

Contingency Factor Breakdown

Item	% of Pressure Mass
Welds and Splices	3.00
Anti-slosh baffles	5.00
Thrust structure	5.85
Forward thrust cone	9.30
Tank support cone	8.80
Tank support/forward thrust cone ring	7.00
Aft Y-ring	14.20
Forward Y-ring	14.20
Aft skirt	8.30
Bottom dome beef-up (thrust)	1.65

5.2 METEOROID PROTECTION REQUIREMENTS

The meteoroid protection system described in Subsection 3.1 employs both the single-wall (armor-plate) and the multi-wall (bumper-shield) concepts. The single-wall requirements serve as the basis for all of the meteoroid protection analyses. Requirements for the multi-wall concept are evaluated by applying an effectiveness factor to the corresponding single-wall requirement. Use of the bare tank wall as meteoroid protection during the one-hour period between the jettisoning of the meteoroid shield and engine ignition is representative of the single-wall requirement. The combination of the interplanetary meteoroid shield and the tank wall for protection during the interplanetary phases is representative of the multi-wall design.

5.2.1 Single-Wall Requirements

The single-wall meteoroid protection requirements are determined by combining an equation describing hypervelocity particle impact with the general expression for meteoroid flux and the definitive parameters of the impacting particles (meteoroid model). Since meteoroids are considered random in occurrence, the perforation equation is presented in the form of the probability of no perforations for a given exposed area-time product and material thickness.

The NASA-MSC Apollo penetration equation given below has been chosen to represent the hypervelocity impact phenomena for this study

$$P = 13.2d^{1/18}\, B_{max}^{-1/3} \left(\frac{\rho_m^{1/3}}{\rho_t}\right)^{1/2} \left(\frac{mV^2}{c_t^2}\right)^{1/3} \qquad (5\text{-}3)$$

This penetration depth is converted to a predicted material thickness at which perforation can just be expected to occur by multiplying Equation 5-3 by a factor of 1.75. By further assuming that the meteoroids are spherical in shape to establish a diameter-mass relationship, the meteoroid mass that just achieves perforation of a thickness, t, can be expressed as

$$m = \frac{t^{2.84}\ \rho_t^{1.421}\ c_t^{1.895}\ B_{max}^{0.947}}{7660\ \rho_m^{0.421}\ V_m^{1.895}} \qquad (5\text{-}4)$$

The meteoroid flux (number of meteoroids of mass m or greater impacting a unit area in a unit time) is generally expressed as

$$\phi = \alpha m^{-\beta} \qquad (5\text{-}5)$$

Substituting the expression for meteoroid mass from Equation 5-4 into Equation 5-5 and multiplying by the product of exposed area and time results in an equation for the expected number of meteoroids that will perforate a specified material thickness and area during the time interval

$$N = \alpha A_E T \left[\frac{t^{2.842}\ \rho_t^{1.421} c_t^{1.895}\ B_{max}^{0.947}}{7660\ \rho_m^{0.421}\ V_m^{1.895}} \right]^{-\beta} \qquad (5\text{-}6)$$

The Poisson distribution is used to predict the number of meteoroids that may be expected to penetrate. Probability of no penetrations is given by the equation

$$N = -\ln P_o$$

or, in the approximate form, (reasonably accurate for $P_o \geq 0.90$)

$$N = 1 - P_o \qquad (5\text{-}7)$$

Equation 5-6 may be expressed in the probability form by substituting the expression for N in Equation 5-7 into Equation 5-6

$$P_o = 1 - \alpha A_E T \left[\frac{t^{2.842}\ \rho_t^{1.421}\ c_t^{1.895}\ B_{max}^{0.947}}{7660\ \rho_m^{0.421}\ V_m^{1.895}} \right]^{-\beta} \qquad (5\text{-}8)$$

The meteoroid parameters (α, β, ρ_m, V_m) as well as the vehicle's transient time and exposed area vary from zone to zone (i.e., near-Earth, interplanetary, and near-Mars).

Theoretically, the total damage to any component should be based on the product of the probabilities of no penetration for the time that the component spends in each zone for both the cometary and the asteroidal fluxes. However, because of the uncertainties associated with the postulated values of the flux, mass, density, and velocity of meteoroids and the untested penetration process at the meteoroid velocities and masses predicted, it was felt that the increased accuracy relative to the complexity was not justified. Therefore, the analysis is based on the use of one set of parameters for the cometary meteoroids and one set of parameters for the asteroidal meteoroids. These parameters are considered to be valid for all of the zones traversed by the vehicle. The total probability of no perforations of a vehicle is the product of the separate probabilities of no perforations for the cometary and the asteroidal meteoroid fluxes.

The meteoroid parameters used in the analysis are presented in Table 5.2-1 for both the cometary and asteroidal meteoroids.

Table 5.2-1 METEOROID PARAMETERS

Parameter	Cometary	Asteroidal
α, number/ft^2-sec (number/m^2-sec)	4.35×10^{-16} (4.68×10^{-15})	3.29×10^{-15} (35.48×10^{-15})
β	1.34	1.0
ρ_m, lb$_m$/ft^3 (gm/cm^3)	31.2 (0.5)	218.5 (3.5)
V_m, mi/sec (km/sec)	13.7 (22.0)	8.1 (13.0)

These data together with the property values for the shield material allow computation of the probabilities from Equation 5-8, for the cometary and asteroidal fluxes, as a function of the product of exposed area and time. Since a specific probability of no perforations of 0.995 is desired, it was necessary to plot the total probability of no perforations versus the exposed area-time product for constant single-wall

thicknesses. From this plot, a cross-plot of single-wall thickness requirements versus exposed area-time for the constant probability of 0.995 was obtained as shown in Figure 5.2-1, with and without the effects of Earth shielding. Earth shielding is based on the assumption that the near-Earth meteoroid flux is isotropic in direction, and thus the Earth would shield the spacecraft from a portion of the flux while it is in the near-Earth zone. An arbitrary 30% reduction in the near-Earth flux was used in this analysis.

5.2.2 Multi-Wall Effectiveness Factors

The bumper or multi-wall requirements for meteoroid protection are obtained by applying the effectiveness factor appropriate to the system design to the single-wall requirements. These effectiveness factors are presented in Figure 5.2-2 (References 3-1 and 5-1). Use of the multi-wall concept in place of the armor method can reduce the mass of the meteoroid protection system while maintaining the same level of protection.

5.2.3 Meteoroid Protection System Mass

The components of the meteoroid protection system have been enumerated in Subsection 3.1. Of the components, only the tank wall and the interplanetary meteoroid shield are affected by the variables in this study. As the tank length increases to accommodate a larger propellant loading or a lower density propellant, the area of both the tank and the meteoroid shield increase.

Meteoroid protection requirements for the tank wall were determined for a one-hour exposure period, using the single-wall meteoroid protection requirements of Figure 5.2-1. In all cases, the wall thickness dictated by the minimum tank design pressure exceeded that required for meteoroid protection.

The interplanetary meteoroid shield is sized by considering a multi-wall system composed of the tank wall and the shield. Nominal tank sizes evaluated from the preliminary analysis provided the area requirements. Tank-wall thickness

for meteoroid protection is known, so that the equivalent single-wall thickness for the shield can be evaluated from the requirements of Figure 5.2-1 and the appropriate effectiveness factor of Figure 5.2-2. Actual sheet thickness of the shield is computed using the three-sheet effectiveness factor from Figure 5.2-2. The meteoroid protection capability of the foam within the shield is included by reducing the three-sheet effectiveness factor from Figure 5.2-2 by a factor of 0.655. Using these sheet thicknesses, the area density of the meteoroid shield (B_{mp} in Equation 6.2-4) can be computed including the low-density foam.

The meteoroid-shield area densities were evaluated for both the Mars Braking and Mars Departure Stages as a function of Mars orbit altitude. These calculations were based on nominal tank areas resulting from the preliminary analysis. Table 5.2-2 presents the values of the area density, which is one of the input quantities to the computer program described in Subsection 6.2.

Table 5.2-2 METEOROID PROTECTION AREA DENSITIES

$$\left[\frac{lb_m}{ft^2} \quad \left(\frac{kg}{m^2}\right)\right]$$

Altitude, n.mi (km)	Mars Braking Stage	Mars Departure Stage
216 (400)	0.643 (3.14)	0.812 (3.96)
3238 (6000)	0.673 (3.29)	0.743 (3.63)
9203 (17,053)	0.691 (3.37)	0.717 (3.50)

Note that the area density increases with altitude for the Braking Stage and decreases with altitude for the Mars Departure Stage, following the general trends in the stage sizes.

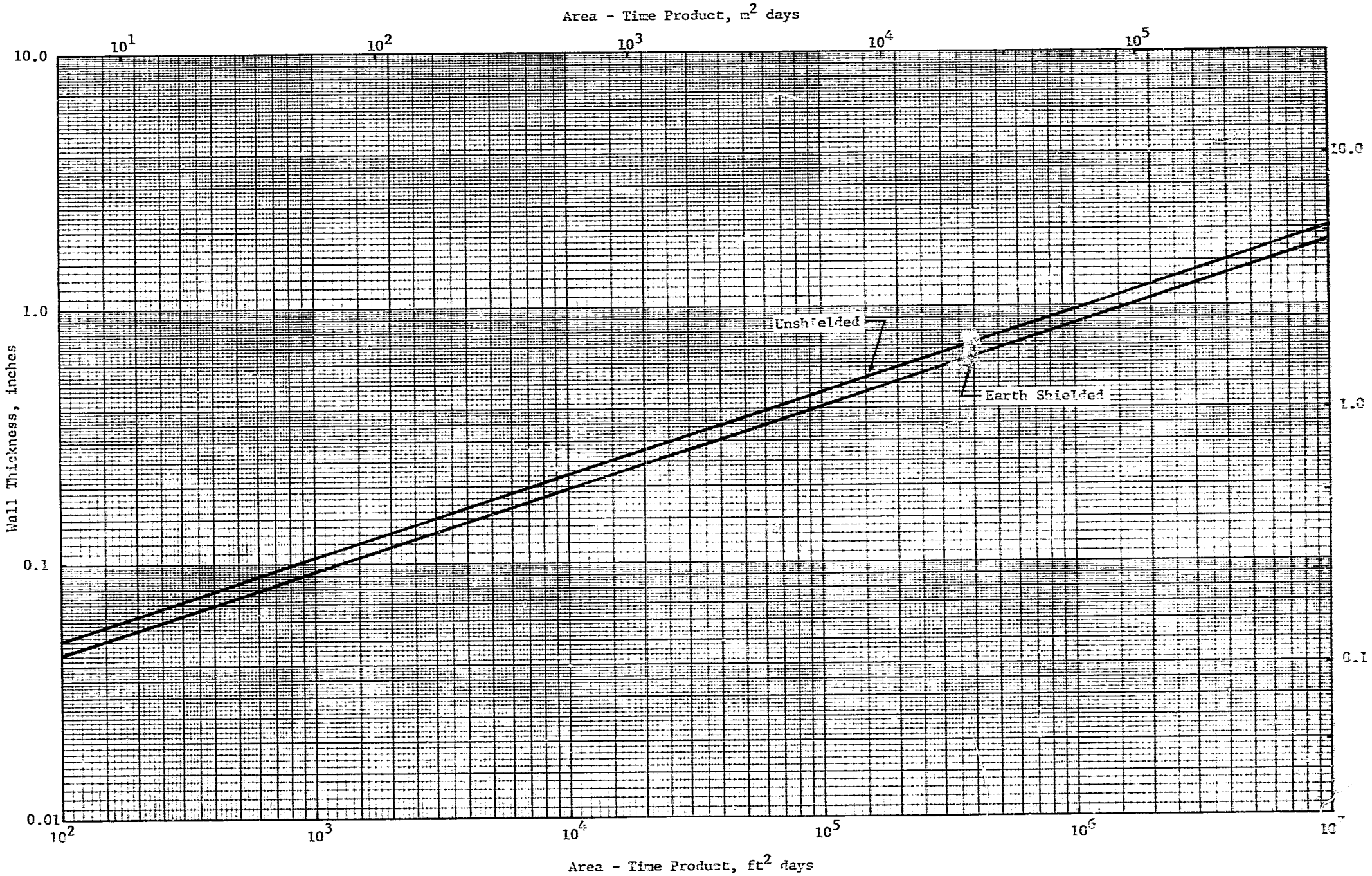

Figure 5.2-1 Single Wall Meteoroid Protection Requirements: $P_o = 0.995$

GENERAL DYNAMICS
Fort Worth Division

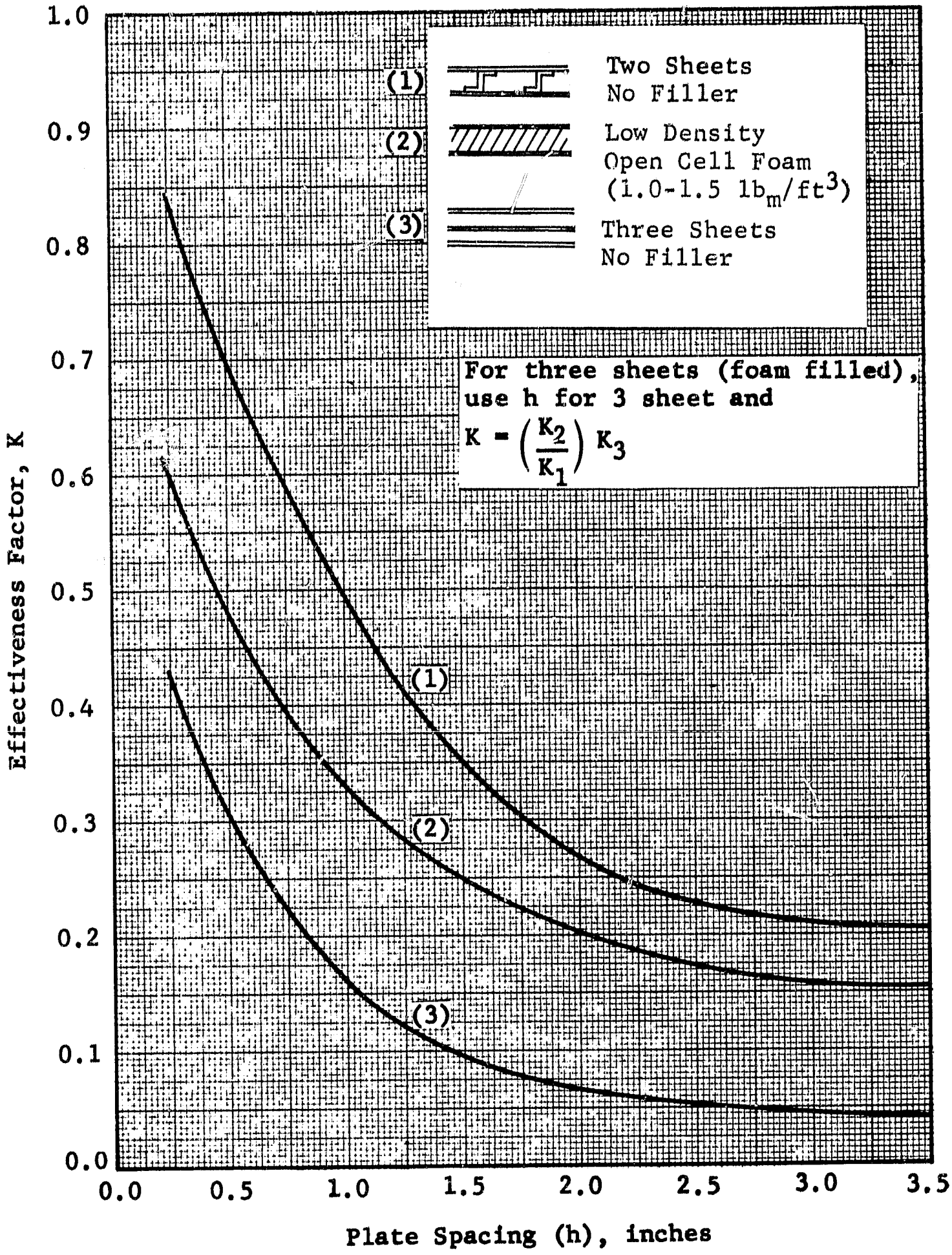

Figure 5.2-2 Multiwall Effectiveness Factors

PRECEDING PAGE BLANK NOT FILMED.

SECTION 6

OPTIMIZATION METHODS

The approach used in this study was based on determination of the optimum propellant storage system for a particular stage of the Mars vehicle. This optimum system is defined in terms of the propellant tank insulation thickness that yields the minimum vehicle IMIEO, with the remaining stages defined in terms of nominal mass fractions. Two different optimization methods were used during the study. In the initial phase, simplified techniques were employed to allow investigation of a wide range of parameters and storage modes, as described in Subsection 6.1. A more complex method was used during the final phase of the study, as described in Subsection 6.2.

Both of the optimization methods are dependent upon the same basic equation for the vehicle IMIEO. The difference in the two methods lies in the simplifying assumptions that are made in order to obtain a solution. The basic equation for the vehicle IMIEO is written in terms of mass fractions for the stage propellant storage system components, with respect to the stage propellant loading.

$$M_o = M_o\,(E_j, A_{1,j}, \ldots A_{j-1,j}, E_{mp_{j-1,j}}) \quad j=1,2,3 \qquad (6\text{-}1)$$

E_j is the mass fraction of the nonjettisoned propellant storage components that are proportional to propellant loading. These items are the propellant tank and related structure whose mass is proportional to tank mass, the insulation, and the pressurant. $A_{k,j}$ is the mass fraction for propellant boiloff vented from the jth stage, during the kth mission phase. The mass of the interplanetary meteoroid shield is represented by the mass fraction, $E_{mp_{j-1,j}}$, which applies to mass jettisoned from the jth stage just prior to engine ignition. In the final analysis, thermal control coating mass is included in the meteoroid protection mass. The coating mass which is not jettisoned is included in the mass of the component on which it is applied.

All of the mass fractions are functions of the insulation thickness so that the minimum IMIEO with respect to an optimum propellant storage system on the jth stage of an

m-stage vehicle is de[illegible] [illegible] ion

$$\frac{\partial M_o}{\partial \delta_j} = 0$$

or

$$\sum_{n=1}^{m} \left[\frac{\partial M_o}{\partial E_n} \cdot \frac{\partial E_n}{\partial \delta_j} + \sum_{k=1}^{n-1} \frac{\partial M_o}{\partial A_{k,n}} \cdot \frac{\partial A_{k,n}}{\partial \delta_j} + \frac{\partial M_o}{\partial E_{mp_{n-1,n}}} \cdot \frac{\partial E_{mp_{n-1,n}}}{\partial \delta_j} \right] = 0 \qquad (6\text{-}2)$$

The mass fractions for a particular stage are a function of the insulation thickness of that stage only. Thus it is possible to reduce Equation 6-2 to the form

$$\frac{\partial}{\partial \delta_j} \left[E_j + \sum_{k=1}^{j-1} \left(\frac{\partial M_o / \partial A_{k,j}}{\partial M_o / \partial E_j} \right) A_{k,j} + \left(\frac{\partial M_o / \partial E_{mp_{j-1,j}}}{\partial M_o / \partial E_j} \right) E_{mp_{j-1,j}} \right] = 0 \qquad (6\text{-}3)$$

Defining the "a factor"

$$a_{k,j} = \frac{\partial M_o / \partial A_{k,j}}{\partial M_o / \partial E_j}$$

and the "d factor"

$$d_j = \frac{\partial M_o / \partial E_{mp_{j-1,j}}}{\partial M_o / \partial E_j}$$

Equation 6-3 can be written as

$$\frac{\partial}{\partial \delta_j} \left(E_j + \sum_{k=1}^{j-1} a_{k,j} \cdot A_{k,j} + d_j \cdot E_{mp_{j-1,j}} \right) = 0 \qquad (6\text{-}4)$$

Further, if E_j is separated into its various components (tank, insulation and pressurant mass fractions) and the mass fractions are written in terms of the mass ratios, Equation 6-4 can be written in the form

$$\frac{\partial}{\partial \delta}\left[\frac{1}{M_H}\left(M_i + M_t + M_p + \sum_{k=1}^{3} a_k \cdot M_{bo_k} + d \cdot M_{mp}\right)\right] = 0 \qquad (6\text{-}5)$$

where the stage subscript, j, has been dropped for simplicity. The insulation thickness that yields the minimum value of the group of terms within the brackets will result in a minimum value of IMIEO. This group is referred to as the "propellant-storage-system effective mass fraction."

Equation 6-5 is the basis of the optimization methods used in this study. In the following subsections, the development of these methods is described further.

6.1 PRELIMINARY ANALYSIS

Since the objective of the preliminary analysis was to perform a rapid, simplified parametric study over a wide range of variables, the task was further subdivided into four parts, corresponding to different propellant storage modes. This allowed a specialized approach to be applied for each mode which permitted considerable simplification of the techniques. The four parts of the analysis were concerned with the nonvent mode, the vent or the partial-recondensation mode, the combination vent-nonvent mode, and the tanking variation of the vent or the partial-recondensation mode. Separate computer programs were developed for each of these analyses. The output quantities from these computer programs are the propellant storage component masses, the propellant tank dimensions, the optimum insulation thickness, the propellant tank wall thickness, the tank pressure and the several mass fractions, including the boiloff mass fractions for each mission phase, for the vent and partial-recondensation modes.

6.1.1 Nonvent Mode

The most obvious characteristic of the nonvent mode is that there is no propellant boiloff and the $\sum a_k M_{bo_k}$ term in Equation 6-5 is therefore zero. A further simplification results from assuming that the mass of propellant contained in the tank is independent of the insulation thickness $\left(\frac{\partial M_H}{\partial \delta} = 0\right)$. The tank mass is calculated from the equation

$$M_t = \frac{\rho_t D^2 F_s F_c}{4 \sigma A_t} \left[\frac{A_o}{2b} + 2\pi(\ell - 2b)\right]\left(P + \rho n \frac{\ell}{2}\right)$$

The coating, insulation, meteoroid protection, and pressurant gas masses may be written as

$$M_c = B_c A_t$$

$$M_i = \rho_i \delta A_t$$

$$M_{mp} = B_{mp} A_{mp}$$

$$M_p = \frac{PV}{0.96 R\overline{T}_{log}}$$

These five masses are all functions of the final propellant specific internal energy, since the propellant density and vapor pressure, and the tank dimensions can all be expressed in terms of the internal energy. This final specific internal energy is defined by

$$u = u_o + \frac{1}{M_H} \sum_k \left[\frac{k\, A_t\, (\overline{\Delta T})_k\, \theta_k}{\delta} + \dot{Q}_{pk}\, \theta_k \right]$$

Since u is a function of the outside surface area of the tank wall, it is necessary to iterate on an initial estimate of u to obtain a solution to Equation 6-5.

Certain assumptions are necessary to facilitate the development of a simple computer program to analyze the nonvent mode. Of primary importance were three curve-fit equations which provided simple, yet accurate, relationships between the specific internal energy of the liquid hydrogen and the saturation vapor pressure, density, and temperature. The saturation pressure is written in the form

$$P_s = (\gamma + Cu)^2 = (12.12 + 1.55u)^2 \quad u < 85 \ \frac{Btu}{lb_m}$$

Thus, it is possible to write the final pressure as

$$P = \Delta P + (\gamma + Cu)^2$$

The saturation liquid density is written as

$$\rho = 4.0 + 0.79 \left(1 - \frac{u}{47}\right)$$

and the saturation temperature is given by

$$T_s = 24.85 + \frac{-1.5217 + [(1.5217)^2 + 0.1326\, u]^{\frac{1}{2}}}{0.06628}$$

These property curve-fit equations are common to all of the preliminary analysis programs and are based on the property data of Reference 6-1. Certain further assumptions, peculiar to the nonvent mode, were necessary to reduce Equation 6-5 to a simple cubic equation. These were $\frac{\partial A_t}{\partial \delta} = 0$ and $\frac{\partial V}{\partial \delta} = 0$. While these assumptions are not strictly correct,

they are very nearly so, since area and volume changes can occur only due to density changes in the propellant, which are, for the most part, small. The reduced form of Equation 6-5 is then

$$\frac{\rho_i A_t \delta^3}{\left(\beta + \frac{V}{0.96\, RT_{log}}\right)} - \delta\left[\gamma + Cu + \frac{C}{M_H}\sum_k \dot{Q}_{pk}\,\theta_k\right]$$

$$\left[\frac{2CKA_t}{M_H}\sum_k (\overline{\Delta T})_k\,\theta_k\right] - 2\left[\frac{CKA_t}{M_H}\sum_k (\overline{\Delta T})_k\,\theta\right] = 0 \qquad (6.1\text{-}1)$$

where

$$\beta = \frac{F_s\, F_c\, \rho_t\, D^2}{4\sigma}\left[\frac{A_o}{2b} + 2\pi(\ell - 2b)\right]$$

Once the mission is defined as to thermal environment and duration, all that is necessary is an initial estimate of the final internal energy. The property curve-fit equations then give the hydrogen properties, from which the tank dimensions are obtained. Equation 6.1-1 is solved for the optimum insulation thickness, and a new value of the final specific internal energy is calculated. This new value is compared to the assumed value of the internal energy. If the assumed and new values are not within ±2 percent, the new value of the internal energy becomes the new estimate, and the procedure is repeated. When the two-percent tolerance is satisfied, the iteration terminates and the output quantities are calculated.

6.1.2 Vent and Partial-Recondensation Modes

The vent and partial-recondensation modes of propellant storage are identical in all respects except for the partial reliquefaction of the propellant vapor in the latter mode. This partial reliquefaction is described mathematically by the use of a fictitious "effective" value of the latent heat of vaporization

$$h_{fg'} = \frac{h_{fg}}{1-r}$$

where r is the fraction recondensed. The same approach may therefore be used for both vent and partial recondensation modes, so that henceforth in this section where "vent mode" is used, one may read "partial-recondensation mode" with equal accuracy.

With the vent mode there is boiloff and all terms in Equation 6-5 are retained. In consequence, it was necessary to assume

$$\frac{\partial M_p}{\partial \delta} = 0$$

$$\frac{\partial t}{\partial \delta} = 0$$

$$\frac{\partial M_{Hu}}{\partial \delta} = 0$$

The use of these assumptions permitted the reduction of Equation 6-5 to the form

$$\delta^2 - \frac{2k\delta}{h_{fg}} \sum_k \eta_k \, (\overline{\Delta T})_k \, \theta_k \frac{\partial A_t}{\partial M_H} - \frac{k}{h_{fg}\rho_i}\Big[(\rho_t t + B_c + dB_{mp}) \sum_k \eta_k \, (\overline{\Delta T})_k \, \theta_k \frac{\partial A_t}{\partial M_H} + \sum_k a_k \eta_k \, (\overline{\Delta T})_k \, \theta_k\Big] = 0 \qquad (6.1\text{-}2)$$

This equation may be solved directly for the insulation thickness, in terms of A_t and η_k, but these are functions of δ, so that it is necessary to begin with initial estimates of A_t and η_k. Using these estimates, a value of the insulation thickness is calculated, from which new values of η_k and A_t are obtained. If the old and new values are not within two percent for η_k and five percent for A_t, the procedure is repeated, using the new values as initial estimates. If the tolerances are met, the iteration terminates and the output quantities are calculated.

6.1.3 Combination Vent-Nonvent Mode

The combination vent-nonvent mode provides a technique for mitigating the effects of extended Earth orbital storage. The combination mode operates by venting excess propellant during the early part of the mission, to allow for expansion of the impulse propellant during the nonvent portion of the mission. For this study, it was considered that the period of vent operation ended prior to the departure from Earth orbit. The solution for the remainder of the mission is identical to that for the nonvent mode, since the starting point is the known vent condition at the end of Earth orbit. It is still necessary to estimate the final internal energy, and the optimization proceeds as described in Subsection 6.1.1. Once the optimum insulation thickness is determined, a check is made to ascertain whether boiloff actually could begin with the calculated optimum insulation thickness, during the time spent in Earth orbit. If boiloff does occur during Earth orbit, the mass of the boiloff and the output values are calculated.

It should be noted that the Earth orbit staytime has no effect on the optimization. This is because the propellant storage system is not altered by the boiloff in Earth orbit, since the excess propellant does not increase the tank size or the impulse propellant requirements. The only effect of longer staytimes and increased boiloff is to increase the IMIEO by the amount of the boiloff.

6.1.4 Tanking Mode

The use of orbital tanking with either the vent mode or the partial-recondensation mode is intended to reduce the effects of the Earth orbit staytime on the stage, and to permit extended Earth orbital storage without penalty. These ends are achieved by allowing propellant which will be needed in the later mission phases to be vented during Earth orbit, and then replenishing the stage from an orbital tanker just prior to Earth departure. Once the vent condition is reached, any additional time in Earth orbit has no effect on the optimization. In this way, all effects of the Earth orbit staytime are removed. After leaving Earth orbit, the conditions are exactly those of the vent (or partial-recondensation) mode.

The program begins by estimating the boiloff after Earth orbit as 20 percent of the impulse propellant, from which the required tank dimensions are calculated. The value of A_t thus obtained is used with $\eta_k = 1$ in Equation 6.1-2 to calculate the optimum insulation thickness. The procedure is repeated using the new tank area as the estimated area until there is less than five percent difference between the old and new values. This fixes the tank size, as well as the initial propellant loading. The energy required to raise the initial propellant mass to the vent condition is then calculated, and compared to the heat transfer during Earth orbit, to determine the time at which boiloff began. Iteration is used to obtain a difference of less than two percent between the required energy and the heat transfer. The Earth-orbit boiloff mass and other output quantities are then calculated.

The mass of propellant which is vented in Earth orbit does not affect the value of IMIEO, since the boiloff is replenished from an orbital tanker.

6.2 FINAL ANALYSIS COMPUTER PROGRAM

The final analysis computer program permitted a more accurate analysis of those cases which were selected for closer examination. This program is described in detail in Reference 6-2. The procedure is a general one, capable of handling all the types of thermal management systems which were examined in the preliminary analysis, including combinations of the vent and partial-recondensation modes with the nonvent mode, and the tanking variation of the vent and partial-recondensation modes.

The program is composed of two distinct sections, a propellant-storage-system optimization section and a mass-buildup section. These sections are used alternately in an iteration procedure to determine the optimum propellant storage system for one stage of the vehicle. The mass buildup section has as its input, stage propellant storage component mass fractions (boiloff, tank, insulation, etc.) and payload masses as well as the various velocity increments, specific impulse, and other mission and vehicle characteristics. The output consists of the vehicle IMIEO, initial stage masses, and various subsystem masses, in particular the propellant loadings, which are obtained from this input data. The propellant-storage-system optimization section has as its input these propellant loadings and thermal environment data and yields the propellant storage component mass fractions, which are returned to the mass-buildup section for the next iteration.

Once the optimum insulation thickness is found, the propellant storage results are printed, with certain pertinent mass buildup information. A final pass through the mass buildup is made, using the optimized mass fractions, to produce the value of IMIEO and the partial derivatives of IMIEO with respect to the various masses and mass fractions. Examples of this output are presented in Volume 3 of this report.

6.2.1 Propellant Storage System Optimization

The propellant-storage-system optimization section of the program, which is essentially the procedure described

in Reference 6-3, is considerably more complex than that of the preliminary analysis. This provides increased accuracy which, when combined with the iteration loops through the mass buildup, results in an accurate analysis of the effects of the stage being optimized on the vehicle IMIEO. Only one stage is considered in the optimization, the others being defined in terms of nominal mass fractions which are used, in conjunction with those produced by the optimization to obtain the IMIEO and the partial derivatives in the mass-buildup section.

The vehicle may have a maximum of six stages and five distinct mission phases, with velocity increments at the beginning and end of each phase. Propellant boiloff and other expendable masses are accounted for in each of these phases. In addition, it is possible to vary the vent energy and the value of the latent heat of vaporization between mission phases. Provision is made to allow tanking of any mode, as well as the venting of excess propellant from a nonvent-mode stage, while in Earth orbit.

Two forms of heat transfer evaluation are available. One is a heating rate applied to the outside of the insulation covering one of nodal areas composing the tank surface; the other is a heating rate applied directly to the propellant. Both are input in the form of tables, as a function of time, and a linear interpolation is performed to obtain an instantaneous rate for numerical integration. The heating rate applied to the propellant is used directly, but an energy balance is required on each node to obtain the temperature drop across the insulation and the resulting heat transfer. This energy balance is of the form

$$\dot{q}_m + \sigma \sum_{j=1}^{n} F_{m-j}\, T_j^{\,4} = \epsilon_m \sigma T_m^{\,4} + \frac{k}{\delta}(T_m - T) \qquad (6.2\text{-}1)$$

where q_m is the surface heating rate obtained from the table and is generally of the form $\left(\frac{\alpha S A_p}{A}\right)_m$.

This energy balance is solved iteratively, and when the surface temperature of each node has been computed, the total energy absorbed by the propellant during the time interval is obtained as

$$\Delta Q = \frac{f\ k\ \Delta\theta}{\delta} \sum_{m=1}^{n} A_m\ (T_m - T) + \dot{Q}_p\ \Delta\theta \qquad (6.2\text{-}2)$$

If the vent energy has not been reached, the specific internal energy of the propellant is calculated

$$u_{\theta + \Delta\theta} = u_\theta + \frac{\Delta Q}{M_H} \qquad (6.2\text{-}3)$$

where M_H is the propellant mass. A nonvent case is one where the vent energy is never reached, so that Equation 6.2-3 is used repeatedly, until the integration is completed at the end of the mission. If the vent energy has been reached, the boiloff mass is

$$M_{bo} = \frac{\Delta Q}{h_{fg}'}$$

where h_{fg}' is an input value equal to $h_{fg}/(1-r)$ and r is the fraction recondensed. The internal energy at the end of the time period is used to obtain the propellant temperature from property tables, and the next step in the integration begins.

When the end of the mission is reached, the tank volume is computed from the equation

$$V = \frac{M_H}{\rho(1 - \mu)}$$

where ρ is the final propellant density, obtained from the final internal energy through property tables, and μ is the ullage volume fraction. Once the volume is known, the tank area is calculated, and compared to the initial value. The new value is then used in the integration, and the process is repeated until the initial and final values agree. The various component masses and mass fractions are then calculated.

The insulation mass fraction is calculated from the total tank surface area and the insulation thickness

$$E_i = \frac{\rho_i \; A_t \; \delta}{M_H}$$

The tank mass fraction is calculated for one of three configurations, as specified in the input data: spherical, cylindrical with hemispherical ends, or cylindrical with ellipsoidal ends. The first two cases use the following equation (spherical tanks have $\ell/D = 1$):

$$E_t = \frac{F_c \; F_s \; \rho_t \; \pi \; D^3}{\sigma \, M_H} \left(\frac{\ell}{D} - \frac{1}{2}\right)\left(P + \rho n \frac{\ell}{2}\right)$$

For the cylindrical tank with ellipsoidal ends, the equation is

$$E_t = \frac{F_c \; F_s \; \rho_t \; D^2}{4 \; \sigma \; M_H} \left[\frac{A_o}{2b} + 2 \; \pi \; (\ell - 2b)\right]\left(P + \rho n \frac{\ell}{2}\right)$$

The meteoroid protection mass fraction calculation also allows for the use of different tank geometries.

$$E_{mp} = \frac{B_{mp}}{M_H}\left[\pi D \; (\ell - 2b) + (1 - n_o)A_o + A_{mp}\right] \qquad (6.2\text{-}4)$$

The coating mass fraction is obtained using a similar equation except that the area density, B_c, and the constant area, A_c, are characteristic of the thermal control coating requirements. Further, the meteoroid protection mass is considered to be jettisoned before engine firing, while coating mass is not. Thus, jettisoned coating may be accommodated by increasing the meteoroid protection area density.

The pressurant-gas mass is obtained from the empirical equation of Reference 6-4.

During the integration, the boiloff mass for each mission phase is recorded, multiplied by the proper "a factor" which accounts for the fact that the boiloff mass is vented from the tank. Similarly, the meteoroid protection mass, since it is jettisoned, has a coefficient, the "d factor", to account for the difference between jettisoned and non-jettisoned mass. The combination vent-nonvent mode and the vent-tanking mode require different treatment of the boiloff which occurs during the Earth

orbit mission phase. For the combination mode, the boiloff in Earth orbit is directly additive to IMIEO, but does not affect tank size, since the volume of boiloff cannot be greater than the expansion volume required for the later mission phases. This mass is defined by the equation

$$M_{Max} = M_H \left(\frac{\rho_{vent}}{\rho} - 1 \right)$$

and is not included in the total effective propellant storage mass fraction. Similarly, the boiloff for the tanking case is taken from propellant which is needed, either for propulsion or boiloff, in later mission phases and is replaced before leaving Earth orbit. This boiloff mass is not included in either the propellant storage mass fraction or the IMIEO.

The total propellant storage effective mass fraction is

$$E_c = E_i + E_t + d \cdot E_{mp} + E_c + E_p + \frac{1}{M_H} \sum_k a_k \cdot M_{bo_k}$$

and this is the quantity in Equation 6-5 which is to be minimized. The value calculated for the particular insulation thickness is compared with that for the previous thickness. Then the insulation thickness is either incremented to the next insulation thickness, or the sign of the increment is changed and the increment halved, depending on whether the previous insulation thickness gave a higher or lower value, respectively, of the total propellant storage effective mass fraction. When the minimum value is found, the non-jettisoned propellant storage system mass fraction, the boiloff fractions, and the meteoroid protection mass fraction are compared to the values which were input to the previous mass buildup. If any one does not agree, the results of the optimization analysis are returned to the mass-buildup section, the mass buildup repeated and the optimization procedure begins again with the masses from the new mass buildup. On the other hand, when all three agree with the previous values, the two output pages are printed, and the mass buildup is entered for a final time, using the results for the optimized case. This gives the final mass distribution of the vehicle.

6.2.2 Mass-Buildup Section

The mass-buildup section of the program serves to compute the IMIEO, the stage component masses, and the mass sensitivities associated with those components. The procedure for the section is identical to that of the mass-buildup program of Reference 6-5. This section requires certain constant performance and mass parameters (specific impulse, thrust-to-mass ratio, velocity increments, payload masses, etc.), for all stages. In addition, fixed component masses and mass fractions for all stages are needed. The nominal mass fractions were used as initial values for the mass buildup. The optimization analysis then supplies updated mass fractions for the particular stage under consideration and the mass-buildup section defines new masses and mass sensitivities for the vehicle, retaining the nominal mass fractions for the propellant storage systems of the non-optimized stages.

The calculations are based on the ideal rocket equation and linear scaling laws for the various subsystems masses.

$$Y = C + E_y M_H \qquad (6.2\text{-}5)$$

where Y is the subsystem mass, C is a constant, and E_y is the mass fraction.

The ideal rocket equation assumes rectilinear motion in force-free space. That is, atmospheric and gravitational effects are neglected, as are those of turning. A need for including any such effects is answered by increasing the velocity increments by appropriate amounts. In particular, for vehicles operated in space, where the primary need is for an allowance for gravity losses due to finite thrusting time, accelerations greater than 0.1 g require only small corrections.

PRECEDING PAGE BLANK NOT FILMED.

APPENDIX A

VENT PRESSURE ANALYSIS

An important consideration in the study was the selection of the vent pressure for the vent and partial-recondensation propellant storage modes. A short study was undertaken, using the preliminary analysis methods, to aid in selecting the vent pressure to be used for both the preliminary and final analyses. In one approach, the tank design pressure is defined as the vent pressure plus a 5 psi (3.45 N/cm^2), increment to allow for the NPSP of the propellant pump and nuclear heating. A second approach was to set the tank design pressure at 28 psia (19.3 N/cm^2), and vary the vent pressure up to a maximum of 23 psia (15.9 N/cm^2). The results of the study are presented graphically in Figure A-1, where the propellant storage system effective mass fraction is shown as a function of the vent pressure for both the vent and partial-recondensation modes.

Two things should be noted about the curves in Figure A-1. When the tank design pressure is fixed, venting at a pressure less than 23 psia (15.9 N/cm^2), that is, the tank design pressure less the NPSP and nuclear heating allowance, results in an increased storage mass fraction and thus a penalty to the vehicle IMIEO. If the tank design pressure is not fixed, a minimum value of the total effective mass fraction occurs for the vent mode at a vent pressure between 13 and 15 psia (8.96 and 10.34 N/cm^2). For the partial-recondensation mode, however, no such minimum exists. The mass fraction increases monotonically with vent pressure. Based on the vent mode results, a vent pressure of 14.7 psia (10.1 N/cm^2) was selected and used throughout the study.

A second series of cases was analyzed using the thermal protection optimization computer program; the results are shown in Figures A-2, A-3, and A-4. Figure A-2 shows trends similar to those of the vent mode in Figure A-1, including a minimum value of the total effective mass fraction in the neighborhood of 14.7 psia (10.1 N/cm^2 abs). The magnitude of the mass fraction is quite different, due to differences in the $k\rho$ value and the analysis methods. Figures A-3 and A-4 present IMIEO and propellant storage penalty data for vehicles with an unshielded Mars Departure Stage and an unshielded Mars Braking Stage, respectively, at the low

altitude. In all cases, both the propellant storage penalty and the vehicle IMIEO show a slight increase as the vent pressure rises.

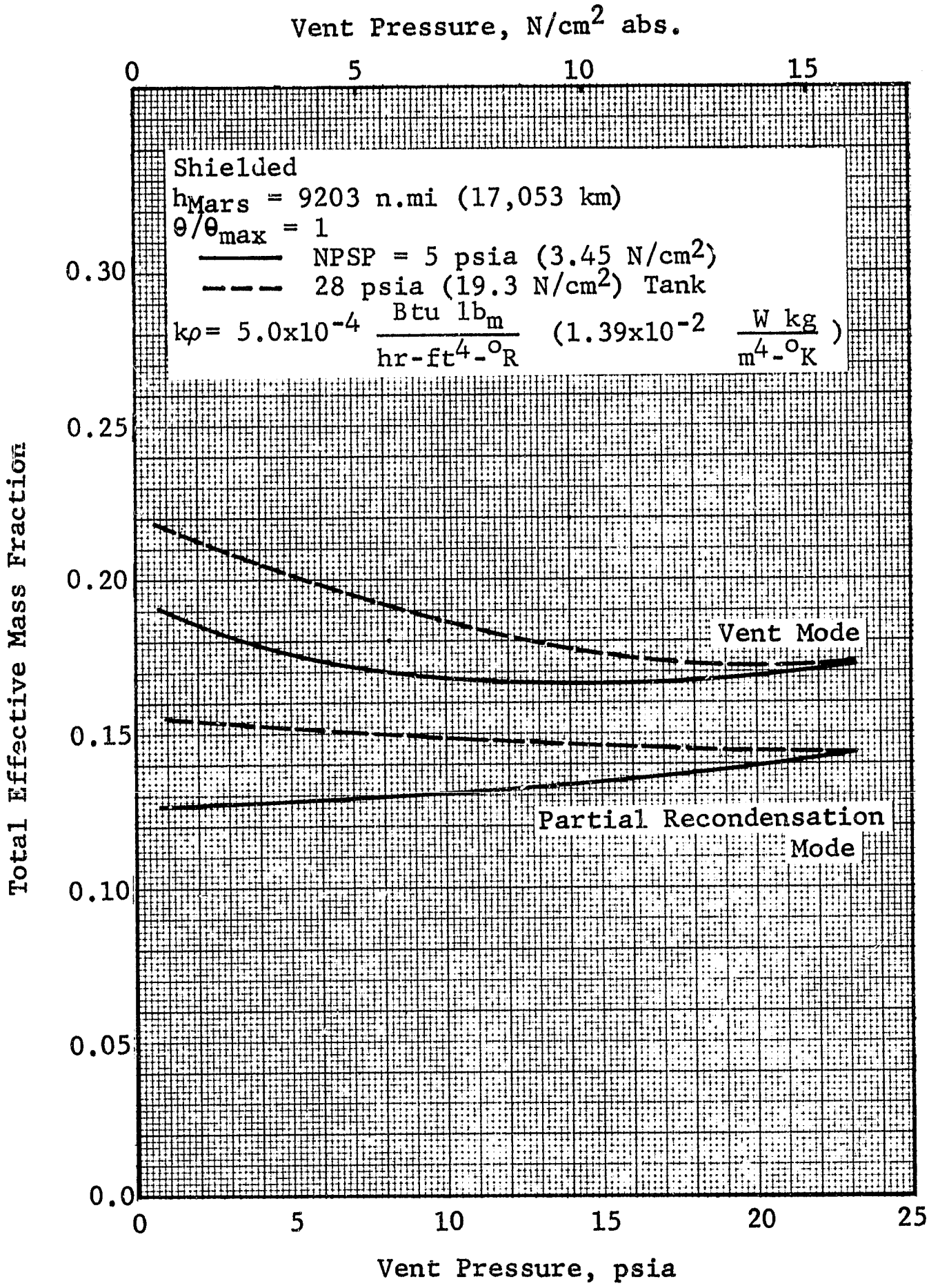

Figure A-1 Effect of Vent Pressure on Optimum Total Effective Mass Fraction: Mars Departure Stage

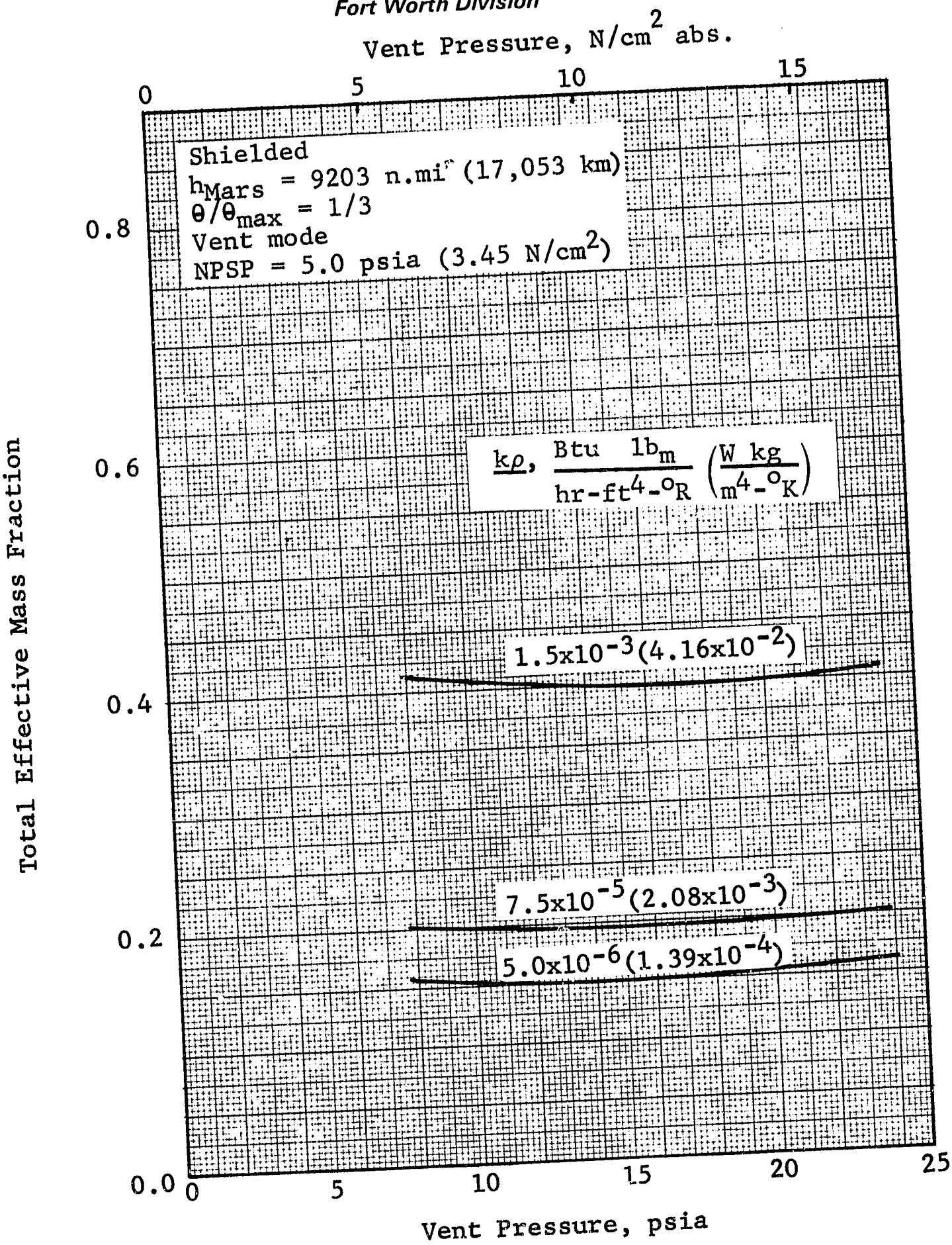

Figure A-2 Effect of Vent Pressure on Optimum Total Effective Mass Fraction: Mars Departure Stage, NPSP = 5.0 psia

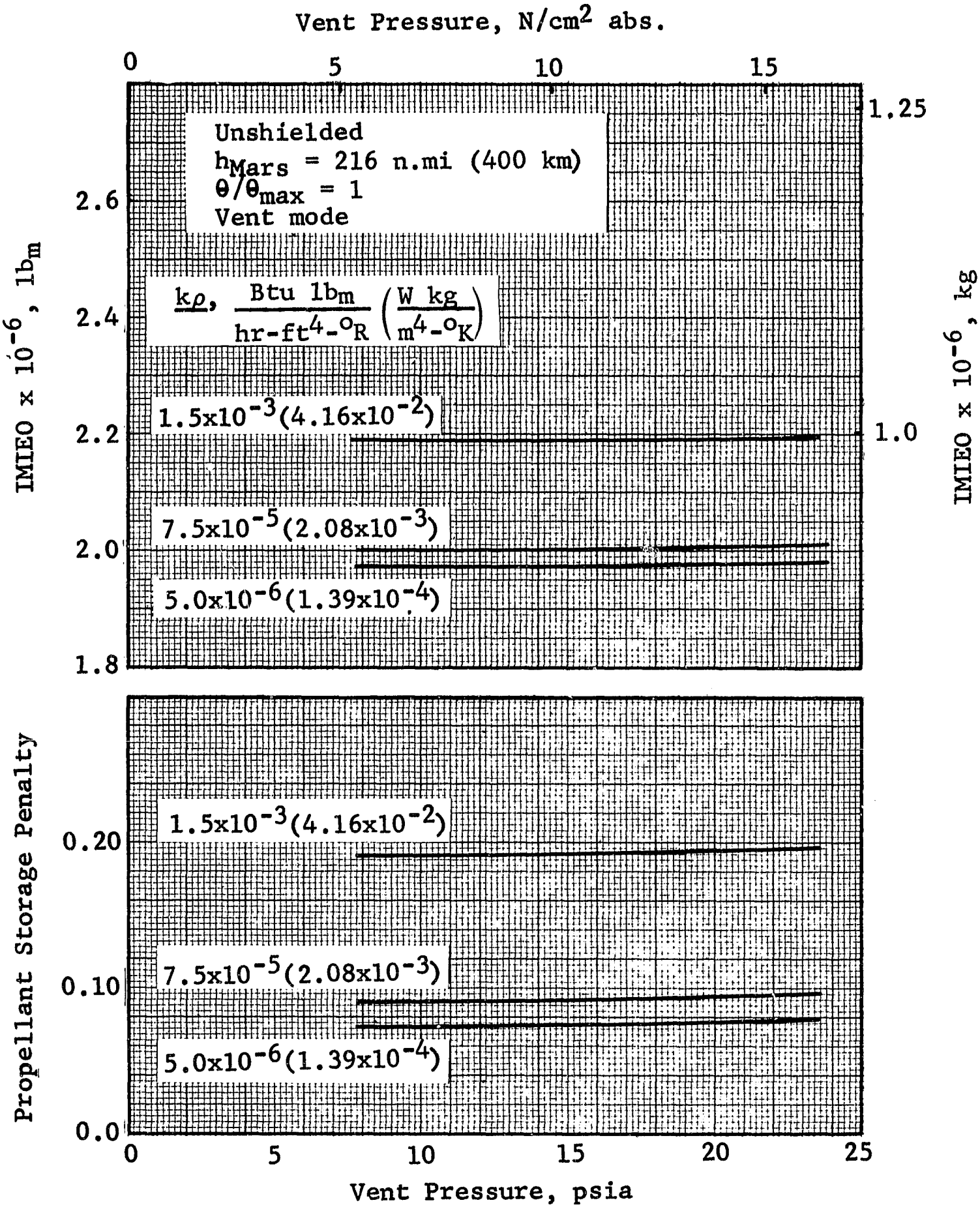

Figure A-3 Effect of Vent Pressure on IMIEO and Propellant Storage Penalty: Mars Departure Stage

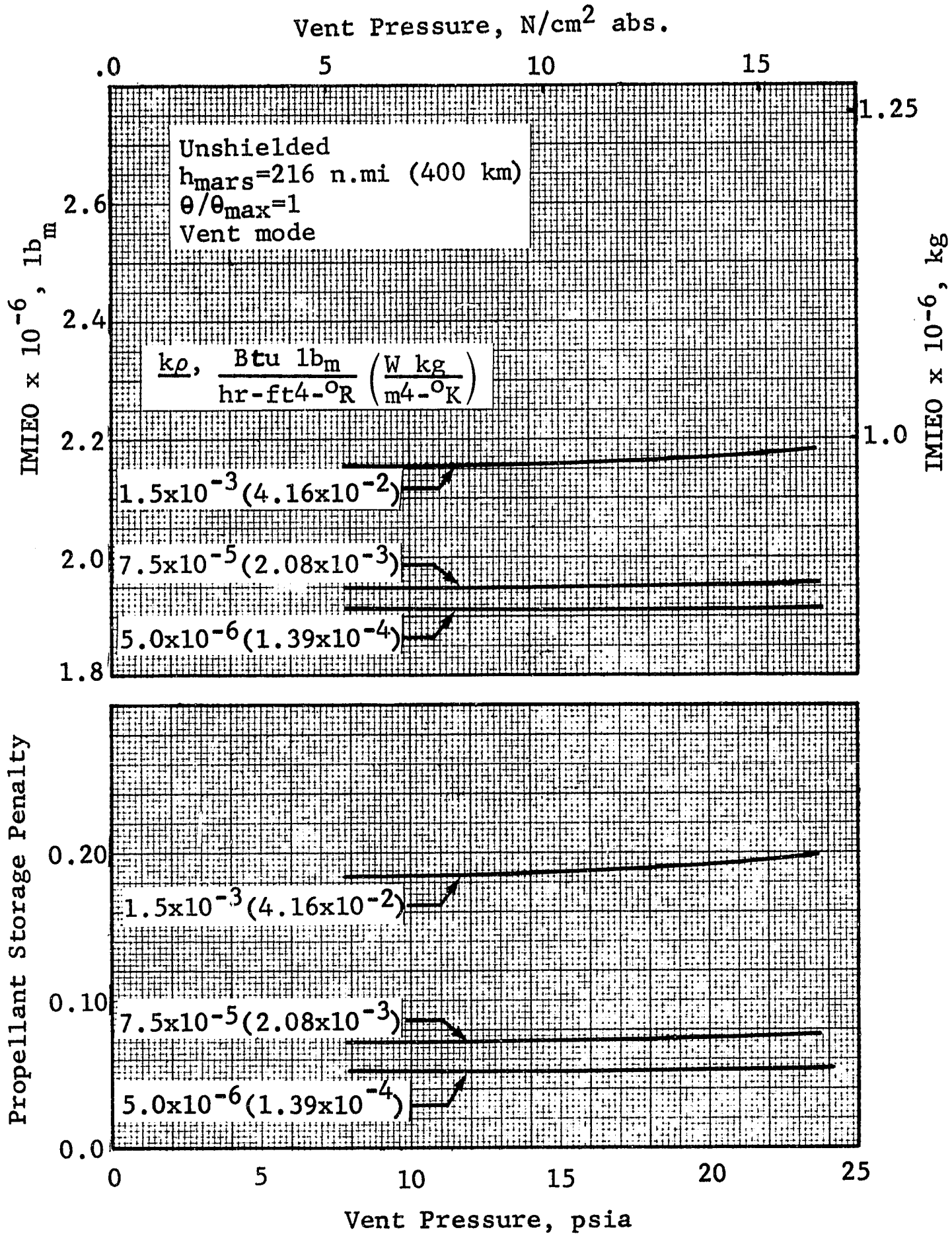

Figure A-4 Effect of Vent Pressure on IMIEO and Propellant Storage Penalty: Mars Braking Stage

APPENDIX B

STRESS ANALYSIS

In order to test the tank design concept, a simplified stress analysis was performed for the critical load conditions. The most severe tension loads occur during Earth launch, when the module is suspended within the ascent shroud by the tank support cone. For this condition, the largest propulsion module represents the worst case. The second critical condition is Earth orbit escape, where the vehicle is completely assembled and the tanks must carry the acceleration loads in compression.

The selection of the module with the critical tension load consisted of selecting the largest Earth Departure Stage propulsion module, since the Earth Departure Stage has the longest propellant tanks. The largest propellant loading occurs with low insulation performance, for the high Mars orbit altitude and vent mode. In addition, an Earth Departure Stage module from a "totally optimized" vehicle was used, since the totally optimized vehicle has more massive upper stages than the nominal upper stages. For the Earth orbit escape condition the more massive upper stages will provide the highest loads, and the most severely loaded module is the Earth Departure Stage propellant module. Therefore, modules of the same Earth Departure Stage represent the critical case for both critical load conditions.

The critical module has a total tank length of 112.4 feet (34.3m). Tank material is 2021-T81 aluminum alloy with an ultimate tensile stress of 70,000 psi (48,300 N/cm^2) at 530°R. A factor of safety of 1.4 was used with the tank design pressure of 19.7 psi (13.6 N/cm^2) to obtain the minimum tank wall thickness of 0.0756 in.(0.192 cm). This thickness occurs at the top of the cylindrical section of the tank, where the tank support cone is attached. The maximum thickness occurs at the bottom of the cylindrical section of the tank, where the tank is joined to the aft skirt. The hydrostatic head at this point is 18.62 psi (12.84 N/cm^2), based on a 6-g acceleration, which together with the design pressure and the 1.4 safety factor gives a maximum wall thickness of 0.147 in.(0.374 cm).

At Earth launch, the entire mass of the module (propellant, tank, engine, interstage structure, etc.) is suspended from the top of the tank. For the critical module this mass is 496,262 lb_m (225,103 kg). In addition, a differential pressure of 2.0 psi (1.38 N/cm^2) is considered to be the minimum required to prevent tank collapse. The stress at the top of the propellant tank is the sum of the stresses due to acceleration and tank internal pressure.

$$f_t = \frac{n\ F_s\ M_{mod}}{\pi Dt} + \frac{F_s\ PD}{4t}$$

$$= \frac{6.0(1.4)(496,262)}{\pi(384)(0.0756)} + \frac{1.4(2.0)(384)}{4(0.0756)}$$

$$f_t = 49,270 \text{ psi}$$

The margin of safety is then

$$M.S. = \frac{\sigma}{f_t} - 1$$

$$= \frac{70,000}{49,270} - 1$$

$$M.S. = +0.42$$

Therefore, the Earth launch condition presents no problem.

For the Earth orbit escape acceleration of 0.4g, the Earth Departure Stage propellant module carries the acceleration loads of all the upper stages in compression. The loads act on the tank at the top of the cylindrical section, where the wall thickness is a minimum. These loads, plus the inertial loading due to the module itself are carried to the lower modules through the aft skirt; both ends of the tank must therefore be analyzed. The tank is pressurized to 19.7 psi (13.6 N/cm^2) at this time which causes a tensile stress in the tank wall.

At the tank support cone attachment point, the stress is merely the difference between the compression stress due to acceleration loads and the tensile stress due to pressurization of the tank. Taking tensile stress to be positive.

$$f = \frac{F_s PD}{4t} - \frac{n\ F_s \sum M_{mod}}{\pi Dt}$$

where M_{mod}, the mass of all modules above the Earth Departure stage, is 1,270,073 lb_m (576,100 kg). Thus

$$f = \frac{1.4(19.7)(384)}{4(0.0756)} - \frac{1.4(1,270,073)(0.4)}{\pi(384)(0.0756)}$$

or

$$f = +27,200 \text{ psi}$$

The margin of safety is then

$$M.S. = \frac{70,000}{27,200} - 1$$

or $$M.S. = +1.57$$

At the lower tank support attachment point it is necessary to consider two additional loads: the compression load due to the mass of the module itself and the hydrostatic head loading. The hydrostatic head is 1.24 psi (0.86 N/cm^2), giving a total internal tank pressure of 20.94 psi (14.44 N/cm^2). The stress is

$$f = \frac{1.4(20.94)(384)}{4(0.147)} - \frac{1.4(1,397,479)(0.4)}{\pi(384)(0.147)}$$

$$f = +14,732$$

Here the 1,397,479 lb_m (633,892 kg) includes the mass of the Earth Departure Stage propellant module. The margin of safety is

$$M.S. = \frac{70,000}{14,732} - 1$$

$$M.S. = +3.75$$

The tank design concept therefore results in a structure that is capable of bearing the expected loads with a substantial margin of safety in all cases.

PRECEDING PAGE BLANK NOT FILMED.

REFERENCES

2-1 Stafford, W. H., et al., Parametric Performance Analysis for Interplanetary Missions Utilizing First-Generation Nuclear Stages, NASA TN D-2160, October 1964.

2-2 Evans, D. E., Pitts, D. E., and Kraus, G. L., Venus and Mars Nominal Environment for Advanced Manned Planetary Mission Programs, NASA SP-3016, 1967.

3-1 Modular Nuclear Vehicle Study Phase II, Vol. III. Nuclear Propulsion Module - Vehicle Design, Lockheed Missiles and Space Company, LMSC-A830246, 1 March 1967.

3-2 McKay, L. M., et al., Study of Conjunction Class Manned Mars Trips, Douglas Missile and Space Division Report SM-48662, June 1965.

3-3 Woodcock, G. R., An Initial Concept of a Manned Mars Excursion Vehicle for a Tenous Mars Atmosphere, NASA TM X-53475, June 1966.

4-1 Greenberg, S. A., et al., "Low Solar Absorptance Surfaces with Controlled Emittance: A Second Generation of Thermal Control Coatings," AIAA Paper No. 67-343, AIAA Thermophysics Specialist Conference, New Orleans, April 1967.

4-2 Ballinger, J. C. and Christensen, E. H., Environmental Control Study of Space Vehicles, Part II. Thermal Environment of Space, Convair Division of General Dynamics Corporation, ERR-AN-016, 10 January 1961.

5-1 Frost, V. C., Aerospace Meteoroid Environment and Penetration Criteria, Aerospace Corporation Report TOR-269 (4560-40)-2, August 1964.

6-1 Keller, C. W., Handbook of Physical and Thermal Property Data for Hydrogen, Lockheed Missiles and Space Company, K-11-67-1, 11 March 1967.

6-2 Barry, D. G. and Hunter, T. S., Integrated Cryogenic Thermal Protection System Optimization and Rocket Vehicle Sizing Analysis, Fort Worth Division of General Dynamics Corporation, ERR-FW-718, 30 December 1967.

6-3 Goodwin, D. W. and Brock, O. R., Thermal Protection Systems for Cryogenic Propellants on Interplanetary Space Vehicles, Vol. III. Analytical Methods, Fort Worth Division of General Dynamics Corporation, FZA-416-III, 21 September 1966.

6-4 Epstein, M., "Prediction of Liquid Hydrogen and Oxygen Pressurant Requirements," Paper No. U-4, 1964 Cryogenic Engineering Conference, Philadelphia, Pennsylvania, August 1964.

6-5 Poteet, M. C. and Wilson, S. W., Jr., General Rocket Vehicle Sizing and Mass Sensitivity Analysis, Fort Worth Division of General Dynamics Corporation, ERR-FW-571, 31 December 1967.